Article

Not peer-reviewed version

A Comparative Analysis of Naïve Exosomes and Enhanced Exosomes with a Focus on the Treatment Potential in Ovarian Disorders

Mohammad Mousaei Ghasroldasht , Farzana Liakath Ali , Hang-Soo Park , Morteza Hadizadeh , Shao Huan Samuel Weng , Allen Huff , Somayeh Vafaei , Ayman Al-Hendy *

Posted Date: 1 April 2024

doi: 10.20944/preprints202404.0003.v1

Keywords: enhanced exosomes; ovarian cancer; polycystic ovary syndrome; poor ovarian reserve; premature ovarian insufficiency

Article

A Comparative Analysis of Naïve Exosomes and Enhanced Exosomes with a Focus on the Treatment Potential in Ovarian Disorders

Mohammad Mousaei Ghsroldasht [1], Farzana Liakath Ali [1], Hang-Soo Park [1], Morteza Hadizadeh [2], Shao Huan Samuel Weng [3], Allen Huff [3], Somayeh Vafaei [1] and Ayman Al-Hendy [1,*]

[1] Department of Obstetrics and Gynecology, University of Chicago, Chicago, IL 60637, USA
[2] Physiology Research Center, Institute of Neuropharmacology, Kerman University of Medical Sciences, Kerman, Iran
[3] Proteomics Platform, Office of Shared Research Facilities, Biological Sciences Division, University of Chicago.
* Correspondence: aalhendy@bsd.uchicago.edu

Abstract: Exosome-based therapy has emerged as a promising strategy for addressing diverse disorders, indicating the need for further exploration of the potential therapeutic effects of the exosome cargos. This study introduces "enhanced exosomes," a novel type of exosomes developed through a novel cell culture system. These specific exosomes may become potent therapeutic agents for treating ovarian disorders. In this study, we conducted a comparative analysis of the protein and miRNA cargo compositions of enhanced exosomes and naïve exosomes. Our findings revealed distinct cargo compositions in enhanced exosomes, featuring upregulated proteins such as EFEMP1, HTRA1, PAM, RSU1, and SDF4, suggesting their potential for treating ovarian disorders. MicroRNA profiling revealed that miR-1-3p, miR-103a-3p, miR-122-5p, miR-1271-5p, miR-133a-3p, miR-184, miR-203a-3p, and miR-206 are key players in regulating ovarian cancer and chemosensitivity by affecting cell cycle progression, cell proliferation, and cell development. We examined polycystic ovary syndrome and premature ovarian insufficiency and identified altered expression of various miRNAs, such as miR-106a-5p, miR-130b-5p, and miR-130b-3p, for diagnostic insights. This study highlights the potential of enhanced exosomes as new therapeutic agents for women's reproductive health, offering a detailed understanding of the impact of their cargo on ovarian disorders.

Keywords: enhanced exosomes; ovarian cancer; polycystic ovary syndrome; poor ovarian reserve; premature ovarian insufficiency

1. Introduction

Extracellular vesicles (EVs), complex structures that are released by cells into the extracellular space, are classified based on their size and biogenesis [1]. These vesicles encapsulate a cytosol devoid of organelles within a lipid bilayer membrane and are thus incapable of replication and coalescing into particles within the submicron range (30–5,000 nm) [2]. The three main classes of EVs are (a) apoptotic bodies, ranging from 800 to 5,000 nm in diameter; (b) microvesicles, also known as shedding MVs, which are large membranous vesicles with diameters ranging from 100 nm to 800 nm; and (c) exosomes, with diameters of 30–160 nm [2,3]. Initially discovered in the 1980s, exosomes were found to have an endosomal origin and are secreted by reticulocytes [4]. Notably, exosomes have a density of 1.13–1.19 g/mL, further distinguishing them as a specific type of EV[5].

Exosomes play a crucial role in intercellular communication and are actively released by various cells, tissues, and bodily fluids such as plasma, urine, saliva, tears, semen, and breast milk [6–12]. Functioning as molecular cargos, these small vesicles contain a diverse array of bioactive molecules, including cytoplasmic proteins, membrane proteins, cytokines, chemokines, cellular receptors, non-coding RNAs, mRNAs, and miRNAs [13,14]. The Vesiclepedia database has a comprehensive

 doi:10.20944/preprints202404.0003.v1

exosomal cargo list that encompasses 566,911 proteins, 27,692 mRNAs, 22,858 miRNAs, 3,839 lipids, and 167 DNAs, emphasizing the extensive and dynamic nature of exosomal content (accessible online: http://microvesicles.org/). Facilitating the intricate exchange of information between cells, exosomes actively engage in the packaging and transportation of molecules. Operating as both paracrine and endocrine signaling agents, exosomes intricately govern cell-to-cell communications, affecting autocrine and paracrine cellular phenotypes [15].

In recent years, exosomes have been studied with a focus on three applications: as diagnostic markers, especially for early detection and screening of cancers [14]; as drug delivery agents [16]; and as therapeutic tools [16]. Influenced by the cell of origin, exosomes contain diverse contents that undergo further variations under distinct physiological and pathological conditions [5]. By Leveraging their nonimmunogenic properties and facilitating passage through biological and physical barriers, exosomes have emerge as promising candidates for delivering tailored molecules to treat specific disorders [17]. The strategic loading of ideal cargo within the lumen or on the surface increase the therapeutic potential of the cargo. Various methodologies, including incubation, transfection of donor cells, and physical treatments such as electroporation, sonication, extrusion, and the chimeric exosome method, have been employed in numerous studies to induce specific small molecules in the exosome lumen, aiming to increase the therapeutic efficacy for specific diseases [18]. However, inducing small molecules may increase the therapeutic efficacy of exosome-based therapy but has limitations. For instance, our knowledge of all small molecules affecting tissue regeneration is incomplete, and even if these small molecules are identified, loading all these small molecules simultaneously in exosomes using current cargo-loading strategies is challenging.

To address this challenge, for the first time, we have introduced a new technique to produce exosomes with a specialized cargo designed specifically for the repair of ovarian disorders. These exosomes, termed enhanced exosomes, are derived from umbilical cord stem cells under unique conditions. In this study, we compared the miRNA and protein profiles of umbilical cord stem cell-derived exosomes (naïve exosomes) and enhanced exosomes, with a focus on the treatment potential in ovarian disorders. This approach aims to provide a targeted and efficient strategy for therapeutic intervention in ovarian disorders, highlighting the potential of exosomes as precision medical tools in the field of regenerative medicine.

2. Materials and Methods

2.1. Cell Culture and Exosome Purification

We utilized mesenchymal stem cells derived from the human umbilical cord (hUC-MSCs) that were obtained from RoosterBio (Frederick, MD, USA). These cells were specifically isolated from the perivascular Wharton's jelly region of the human umbilical cord. The cultivation and expansion of these cells adhered to the guidelines provided by RoosterBio and were conducted in RoosterNourish-MSC-XF medium (RoosterBio, Frederick, MD, USA) until the cells reached 80% confluence. After reaching the third passage at 80% confluence, the hUC-MSCs were washed three times with phosphate-buffered saline (PBS) and subsequently cultured with RoosterCollect-EV Pro™ medium (RoosterBio, Frederick, MD, USA) for 48 hours. The resultant culture medium, enriched with secreted exosomes, underwent a series of centrifugation steps: 500 × g for 5 minutes at 4 °C to eliminate cell debris, followed by 2000 × g for 20 minutes to remove apoptotic bodies, and 10,000 × g for 30 minutes to exclude microvesicles. The purification of exosomes was performed with the poly-ethyl glycol (PEG)-based precipitation method (ExoQuick-TC, System Biosciences, CA), which strictly adhered to the manufacturer's protocol. Briefly, 1 ml of ExoQuick-TC was added to 5 ml of culture media, and the mixture was incubated overnight at 4 °C. The ensuing centrifugation at 1,500 × g for 30 minutes resulted in the pelleting of exosomes. The resulting pellet was resuspended in 200 µl of PBS, and the quality and quantity of the exosomes were evaluated using NanoTracking Particle analysis with a NanoSight NS300 system (Malvern Panalytical, United Kingdom). The purified exosomes were stored at -80 °C and subjected to no more than one freeze-thaw cycle.

 doi:10.20944/preprints202404.0003.v1

The immortalized human granulosa cell line (HGrC1), a generous gift from Dr. A. Iwase (Nagoya University, Japan), was cultured in DMEM-F12 supplemented with 10% fetal bovine serum, and 1% penicillin-streptomycin (Thermo Fisher Scientific Inc., MA, USA).

To produce enhanced exosomes, we cultured hUC-MSCs with HGrC1 cells in accoedance with a system protected by intellectual property rights (patent number: PCT/US2022/073467). The culture medium enriched with exosomes was harvested and subjected to a series of sequential centrifugation steps: centrifugation at 500 × g for 5 minutes, 2000 × g for 20 minutes, and 10,000 × g for 30 minutes to eliminate debris, apoptotic bodies, and microvesicles, respectively. Exosome purification was carried out using ExoQuick-TC, strictly following the manufacturer's instructions. The quality and quantity of the exosomes were thoroughly analyzed using a NanoSight NS300 system.

To validate the distinctive morphology of both naïve exosomes and enhanced exosomes, we performed transmission electron microscopy (TEM) studies. In brief, exosomes were applied to a copper mesh grid coated with a carbon film for 1 minute and subsequently negatively stained with 0.75% uranyl formate for 45 seconds. After the drying process, TEM imaging was conducted using an FEI Tecnai G2 F30 system operating at 300 kV. Western blot analysis, based on the manufacturer's protocol, was used to validate the presence of exosomal markers, including CD9, CD63, and CD81 (System Bioscience, USA).

2.2. Proteomics

2.2.1. Chemicals and Reagents:

Tris(2-carboxyethyl)phosphine (TCEP; C4706), iodoacetamide (IAA; I6125), and calcium chloride (C5080) were obtained from Sigma. Ammonium bicarbonate (BP2413), LC-MS grade acetonitrile (A955-4), and water (W6-4) were obtained from Fisher Scientific. Formic acid (cat. no. 94318) was sourced from Honeywell. Trypsin/LysC (sequencing grade; Promega; V5073) was obtained.

2.2.2. S-Trap Digestion Protocol:

Protein extraction was conducted from 40 billion particles of both naïve exosomes and ovarian-specific exosomes. For this procedure, exosome samples in PBS were denatured using equal volumes of 2×S-Trap lysis buffer (10% SDS, 100 mM TEAB, pH adjusted to 7.55 using 12% phosphoric acid). The samples were subjected to bead beating and reduction with 20 mM TCEP (200 mM TCEP in 770 mM TEAB, pH 7.8) at 65 °C for 30 min. Subsequently, the reduced proteins were alkylated with 80 mM iodoacetamide in the dark for 30 min at room temperature. Acidification of the samples was performed using 12% phosphoric acid (final concentration 1.2%), followed by dilution with a 6× volume of S-Trap binding buffer (methanol containing 100 mM TEAB, pH adjusted to 7.2 using 12% phosphoric acid). The diluted sample was loaded onto an S-Trap micro column using a microcentrifuge with a flow-through waste collector. Finally, SDS was completely eliminated from the sample by washing the filter three times with 160 µL of S-Trap binding buffer. The purified protein samples on the filter were then subjected to digestion using 2 µg of trypsin/Lys-C (#V5073, Promega) in 50 mM ammonium bicarbonate and 0.5 mM CaCl2 at 37 °C overnight. The digested peptides were collected by washing the filter in three steps with 40 µL of 50 mM ammonium bicarbonate, 40 µL of 0.15% formic acid, and 40 µL of 0.15% formic acid in 60% acetonitrile. The eluate was dried in vacuo and stored at −80 °C prior to analysis.

2.2.3. LC-MS Parameters:

The samples were analyzed with an Exploris 480 mass spectrometer along with an UltiMate 3000 liquid chromatography system (Thermo Scientific). A MonoCap column from GL Sciences, measuring 50 cm in length and 0.75 mm in inner diameter (Cat. No. 5020-10006), was used, with a flow rate of 500 nL/min and a constant temperature of 25 °C.

For the analysis, mobile phase A (0.15% formic acid in water) and mobile phase B (0.15% formic acid in 100% acetonitrile) were used. The gradient spanned 130 minutes: 5% B for 5 minutes,

 doi:10.20944/preprints202404.0003.v1

transitioning from 5% to 22% B over 100 minutes, followed by a shift from 22% to 34% B over 19 minutes, and a rapid transition from 34% to 95% B in 1 minute. The mixture was held at 95% B for 5 minutes.

A full-scan MS spectrum ranging from 350 to 1650 m/z was collected at a resolution of 60,000 at m/z 200. The maximum injection time was set to 50 ms, with an AGC target value of 3e6. The cycle time for data acquisition was set to 3 seconds, and the intensity threshold was set at 5e4.

For MS/MS scans, a resolution of 15,000 was utilized, with the maximum acquisition time set to auto and an AGC target value of 4e4. The isolation window at the Orbitrap cell was set to 1.6 m/z, and the first mass was set to 110 m/z. The collision energy for HCD was set to 32. A dynamic exclusion duration of 30 seconds was implemented. Charge states 2 to 7 were included, while unassigned charge states were ignored. The heated capillary temperature was set to 300 °C.

2.2.4. Proteomics Analysis:

Raw MS data were processed and searched using Proteome Discoverer (version 3.0.0.757; Thermo Fisher Scientific) with the Sequest HT search engine. A precursor mass tolerance of 10 ppm and fragment mass tolerance of 0.02 Da were applied. The human database was downloaded from UniProt.

A 1% FDR cutoff, estimated by Percolator, was applied to filter the data. Trypsin (full) was used as the enzyme, with a maximum of 3 mass cleavages, and peptide lengths ranging from 4 to 45. Carbamidomethyl (+57.021 Da on C) was selected as a fixed modification, while oxidation (+15.995 Da on M), deamidated (+0.984 Da on N and Q), protein N-terminal Met-loss (-131.040 Da), acetyl (+42.011 Da on N-terminus), and protein N-terminal Met-loss+acetyl (-89.030 Da) were considered dynamic modifications.

Gene set enrichment analysis (GSEA) provides crucial insights into the biological functionality of organisms, focusing on Gene Ontology (GO) and biological pathway analyses. The GOplot and ClusterProfiler packages in R software allow a thorough examination of the final list, facilitating a comprehensive investigation of both GO and pathway enrichment. The analysis was performed with a significance threshold of P.adjust < 0.05, ensuring that only the most statistically significant outcomes were considered.

2.3. MiRNA Sequencing

RNA was extracted from 40 billion particles of both naïve exosomes and enhanced exosomes using the SeraMirTM Kit (System Biosciences, CA) following the manufacturer's protocol. Following a rigorous quality control assessment of the isolated RNA, a small RNA sequencing assay was carried out by Novogene Company (San Diego, CA, USA) in accordance with the established protocol (Novogene mRNA-seq Services).

In essence, 3' and 5' adaptors were ligated to the respective ends of small RNAs, and first-strand cDNA was synthesized after hybridization with the reverse transcription primers. The resulting double-stranded cDNA library was generated through PCR enrichment. After purification and size selection, libraries with insertions ranging from 18 to 40 bp were prepared for sequencing on Illumina platforms with PE50.

Quantification and size distribution analysis of the libraries were performed using Qubit, real-time PCR, and bioanalyzer methodologies. Subsequently, the quantified libraries were pooled and subjected to sequencing on an Illumina platform, determined by the effective library concentration and the requisite data volume. The bioinformatics team at Novogene conducted a thorough analysis involving the mapping and identification of known miRNAs using Bowtie (version 1.0.1) and mirDeep2, respectively. Novel miRNAs were predicted through miREvo (version MirEvo_v1.1) and mirDeep2. For animal target prediction, miRanda (version miRanda-3.3a) and RNAhybrid (version RNAhybrid v2.0) were used. Additionally, GO and KEGG enrichment analyses were carried out using clusterProfiler (version 3.8.1) with the parameter padj <0.05.

 doi:10.20944/preprints202404.0003.v1

3. Results

3.1. Exosome Characteristics:

Extracellular vesicles in their original state were obtained from human umbilical cord mesenchymal stem cells (hUC-MSCs) cultured under conventional conditions, while enhanced exosomes were harvested from hUC-MSCs exposed to unique conditions. Nanoparticle tracking analysis (NTA) revealed that the particle size ranged from 30 to 200 nm, with an average size of 109.9 nm for naïve exosomes and 94.9 nm for enhanced exosomes (Figure 1). Notably, the concentration of enhanced exosomes was greater than that of naïve exosomes for the same number of seeded cells, indicating that the cells cultured in our new cell culture system secreted more particles (1.04e+10 particles/ml naïve exosomes versus 4.11e+10 particles/ml enhanced exosomes). The morphology of the isolated exosomes was evaluated using TEM, which revealed no discernible differences in shape between the naïve and enhanced exosomes. Western blotting analysis confirmed the expression of exosomal marker proteins, including CD9, CD63, and CD81 (System Bioscience, USA), in both naïve and enhanced exosomes.

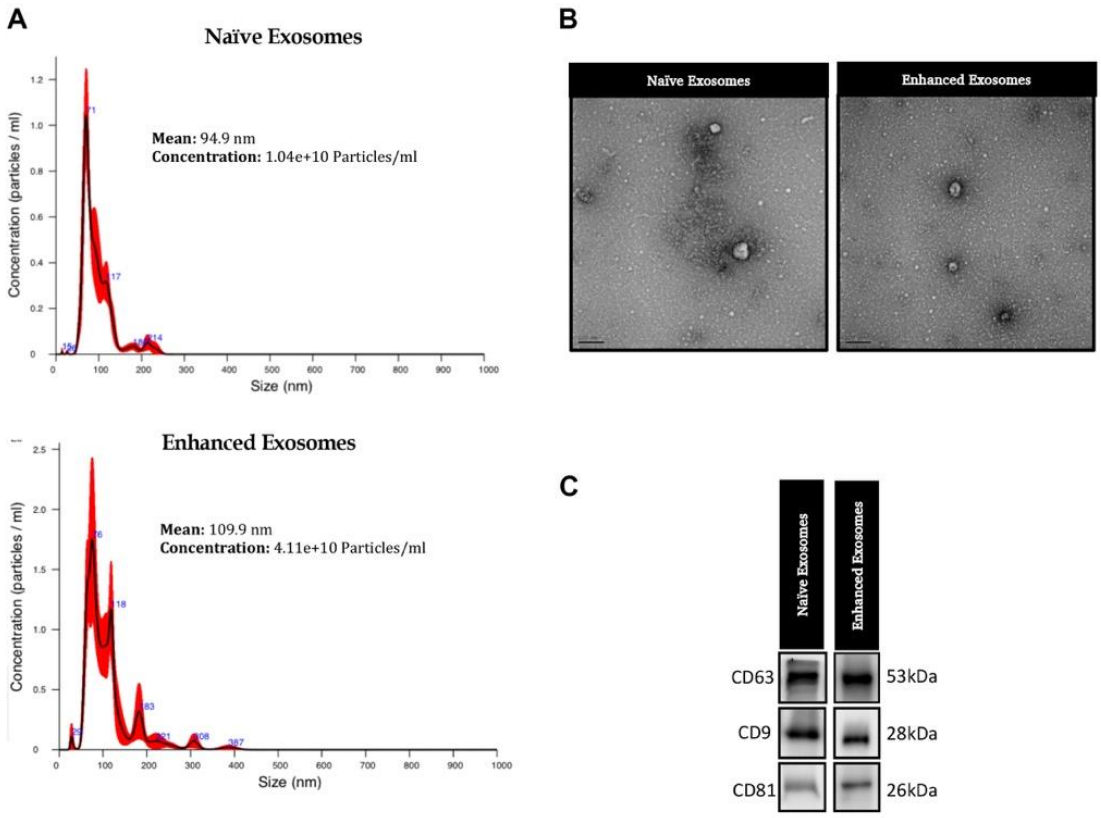

Figure 1. Characterization of exosomes derived from umbilical cord mesenchymal stem cells under conventional conditions (naïve exosomes) and specific cell culture conditions (enhanced exosomes). A) Nanoparticle tracking analysis (NTA), revealing the average size and number of particles. B) Transmission electron microscopy (TEM) images illustrating the morphology of naïve and enhanced exosomes. C) Western blot (WB) analysis of exosomal markers (CD63, CD9, and CD81) in naïve and enhanced exosomes.

3.2. Bioinformatics Analyses of Proteins Derived from Naïve Exosomes and Enhanced Exosomes

A comparison between naïve exosomes and enhanced exosomes is presented in Figure 2a; a volcano plot was used to show the variations in protein expression between each pair of groups. The proteins were categorized into three groups: all proteins, extracellular vesicle-specific proteins, and

 doi:10.20944/preprints202404.0003.v1

exosome-specific proteins. A chord plot and cnetplot were generated to identify enriched genes and pathways according to the Gene Ontology (GO) and KEGG enrichment analyses, with an adjusted P value <0.05. Like enhanced exosomes, naïve exosomes contained proteins involved in the generation of precursor metabolites and energy and ribonucleoprotein complex biogenesis in the biological process category (Figure 2b). For cellular components, both naïve and enhanced exosomes were associated with cell-substrate junctions and focal adhesions. In terms of molecular function, cadherin binding was the primary function for both types of exosomes in all protein categories (Figure 2b).

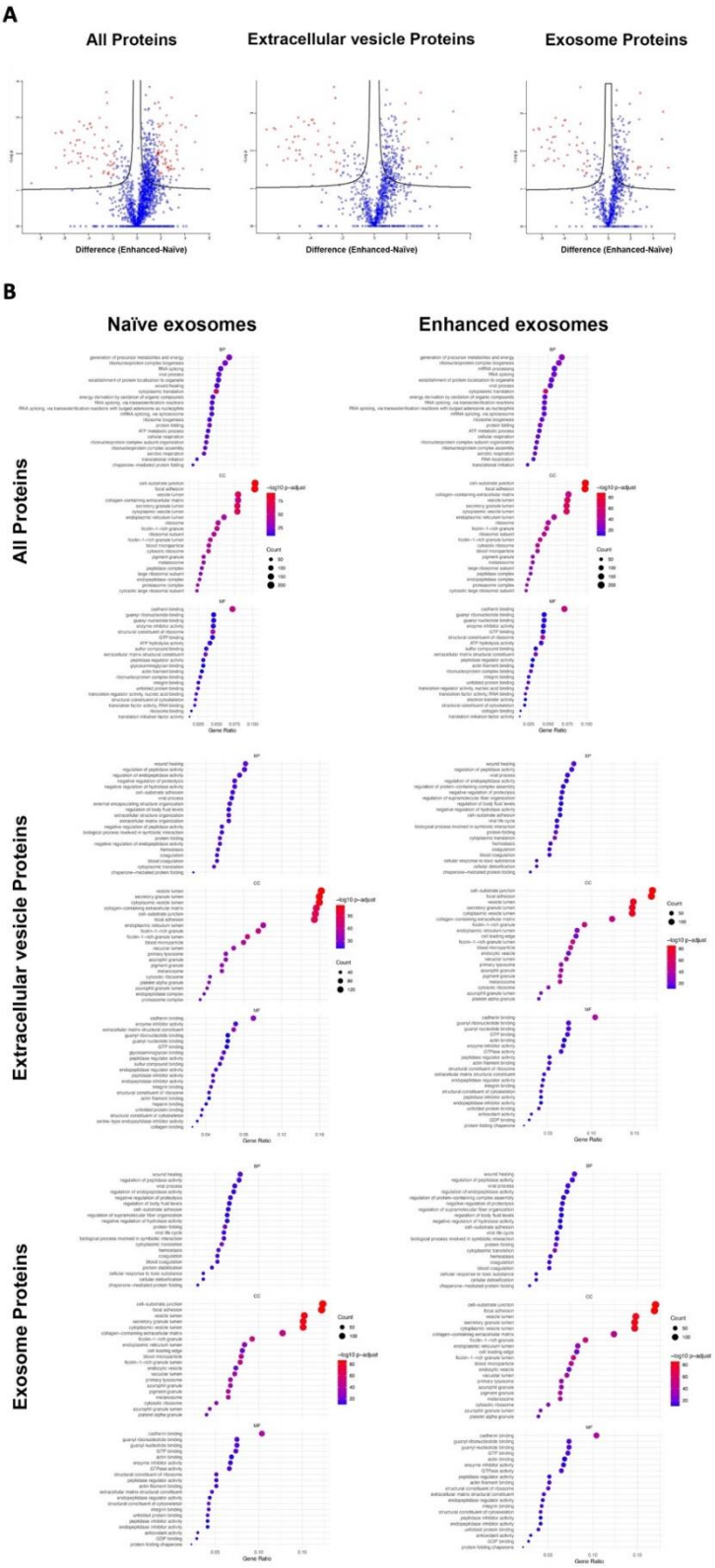

 doi:10.20944/preprints202404.0003.v1

Figure 2. Protein analysis of naïve exosomes and enhanced exosomes. A) Volcano plots of log2 fold changes (x-axis) and their associated -log10 transformed P-values (y-axis) for all identified proteins, extracellular vesicle proteins and exosome proteins. B) GO analysis of all the identified proteins, extracellular vesicle proteins and exosome proteins in the naïve and enhanced exosome groups.

In the extracellular vesicle protein category, both naïve and enhanced exosomes played roles in wound healing and the regulation of peptide activity in biological processes. Cadherin binding was a significant molecular function for both groups. However, in cellular components, naïve exosomes had more proteins involved in vesicle lumen and secretory granule lumen, while enhanced exosomes had more proteins involved in cell-substrate junction and focal adhesion (Figure 2c). In the exosome category, the proteins associated with biological processes, cellular components, and molecular functions were consistent between the naïve and enhanced exosome groups (Figure 2d).

To further elucidate the differences between enhanced and naïve exosomes, we compared the expression of proteins significantly overexpressed in the enhanced exosomes. There were 191 proteins significantly overexpressed in all protein categories, 91 in the extracellular vesicle category, and 72 in the exosome category (Supplementary data, Table S1). According to the analysis of all protein categories, the GO analysis revealed involvement in biological processes such as RNA splicing and mRNA processing (Figure 3A). In terms of cellular components, there was a greater representation of proteins associated with the collagen-containing extracellular matrix, while the molecular functions were predominantly related to the extracellular matrix structural constituent (Figure 3A). In the extracellular vesicle category, proteins were linked to biological processes involving extracellular structure organization, extracellular matrix organization, and external encapsulating structure organization. The collagen-containing extracellular matrix dominated the cellular component, and the molecular function was primarily associated with extracellular matrix structural constituents (Figure 3a). Within the exosome category, proteins shared similarities with those in the protein and extracellular vesicle categories in terms of cellular components and molecular functions. However, proteins in this category play specific roles in the regulation of mRNA splicing and mRNA processing within biological processes (Figure 3a). KEGG pathway analysis revealed predominant enrichment in the cell cycle for all proteins in the enhanced exosome group (Figure 3b), with additional pathways such as the PI3K-Akt signaling, AMPK signaling, apoptosis, RNA transport, cGMP-PKG signaling, mTOR signaling, and DNA replication pathway being significantly overexpressed in the enhanced exosome group compared to the naïve exosomes group (Supplementary data, Table S2).

Preprints.org (www.preprints.org) | NOT PEER-REVIEWED | Posted: 1 April 2024 doi:10.20944/preprints202404.0003.v1

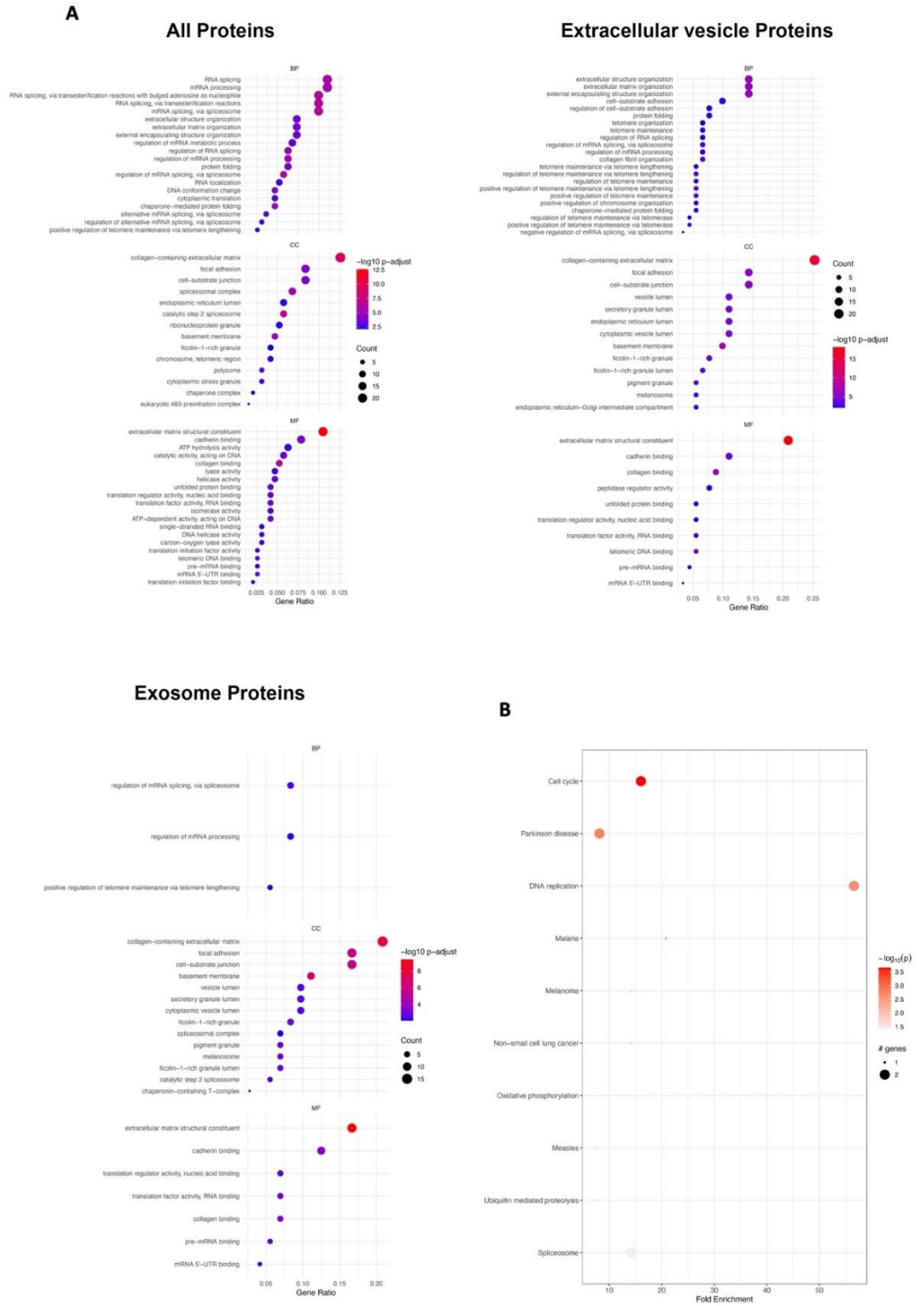

Figure 3. Protein analysis of proteins significantly overexpressed in enhanced exosomes. A) GO analysis of all the identified proteins, extracellular vesicle proteins and exosome proteins. B) KEGG pathway.

3.3. Bioinformatics Analyses of miRNAs Derived from Naïve Exosomes and Enhanced Exosomes

A venn diagram describing the miRNA profile of naïve exosomes versus enhanced exosomes indicated the presence of 487 common miRNAs, 183 miRNAs unique to naïve exosomes, and 101

 doi:10.20944/preprints202404.0003.v1

miRNAs unique to enhanced exosomes (Figure 4A). To assess the notable differences between the two exosomal miRNAs, we generated a volcano plot to identify the uniquely expressed or overexpressed miRNAs in each group (Figure 4B). The data revealed that 34 miRNAs exhibited significant upregulation in the enhanced exosomes compared to the naïve exosomes, while 74 miRNAs displayed significant downregulation in the enhanced exosomes in comparison to the naïve exosomes (fold change >2, and P-value <0.05, see Supplementary Table S3 for a complete list). Given that each miRNA can target several genes, influencing their expression or translation, these diverse miRNAs likely to play roles in various crucial mechanisms related to ovarian regeneration. Table 1 provides an overview of the target genes of a selection of well-known miRNAs that are overexpressed in enhanced exosomes compared to naïve exosomes (the network of miRNAs and target genes is illustrated in Supplementary Figure S2.)

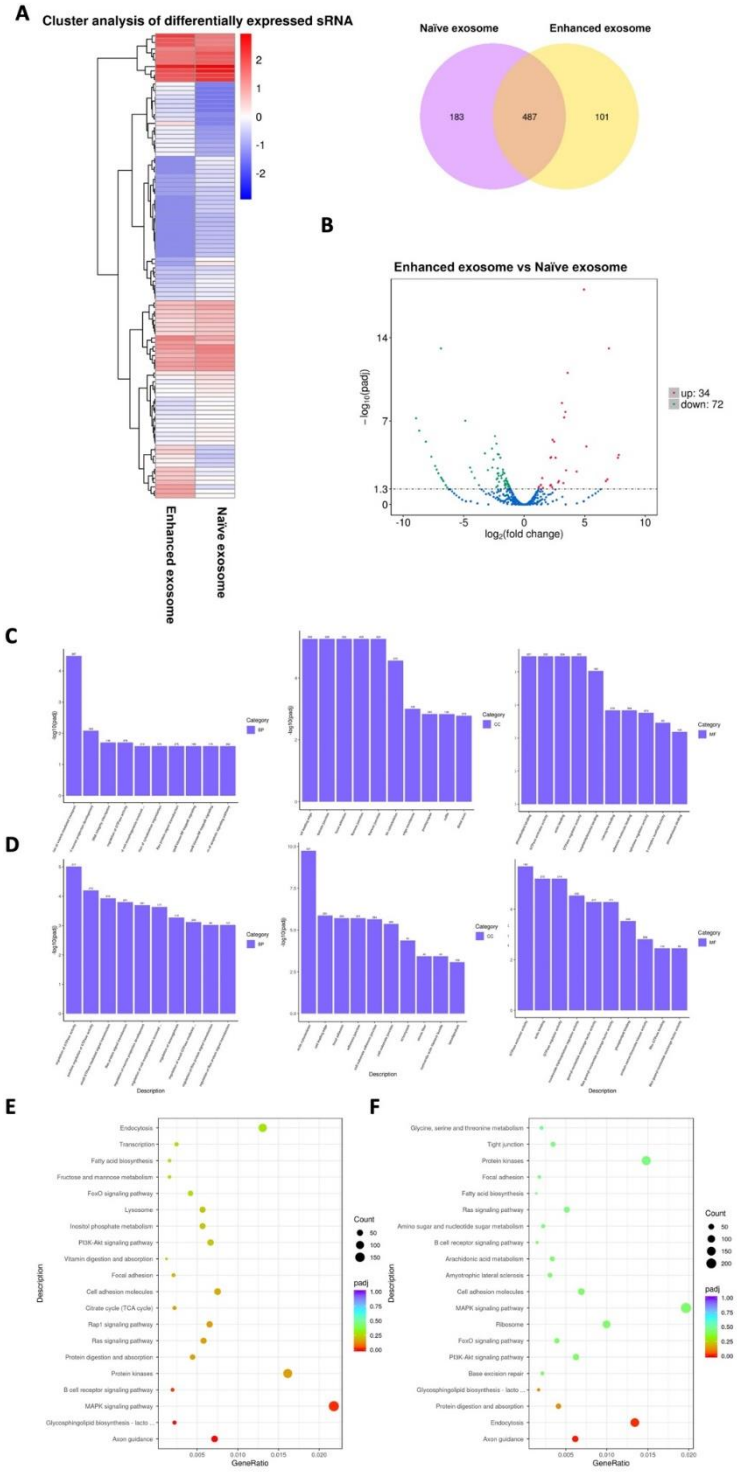

 doi:10.20944/preprints202404.0003.v1

Figure 3. MiRNA analysis of naïve exosomes and enhanced exosomes. A) Heatmap and Venn diagrams of the miRNA levels in naïve and enhanced exosomes. B) Volcano plots of log2 fold changes (x-axis) and their associated -log10 transformed P-values (y-axis) for all identified miRNAs. C) GO analysis of all the detected miRNAs. D) GO analysis of miRNAs significantly upregulated in the enhanced exosomes. E) KEGG analysis of all the detected miRNAs. F) KEGG analysis of miRNAs significantly upregulated in the enhanced exosomes.

Table 1. Target genes of each miRNA.

[redacted]	
hsa-miR-103a-3p	IL32,P4HA2,DRD4,TMEM101,TEKT2,PPP6R2,PLEK2,CHGA,USP11,PEX11G,NOD1,HSD17B1,PPY,OSCP1,TBX4,FBXO24,POLM,ITPR2,UBE2C,WFDC3,PACSIN1,DDX49,ANGPTL8,MYBPH,MORC4,OS9,SQOR,SLC3A1,VSX2,CCNE1,MOV10L1,SIRPB1,SEMA3A,HPX,ETNK1,ITGAX,NDUFB10,DEF8,ZNF750,SIK1,SLC44A3,REG3G,GPR6,HIKESHI,CC2D1B,OBSCN,GSTT2B,SPON2,PIP,SSU72,OLFML2B,BOLA3,ZDHHC19,FBXW12,SERPINA4,TMED3,PHB,DEFB4A,WDR48,UMOD,ANKS3,DISP3,EXOSC10,PTCRA,REG3A,MTCL1,C17orf62,AVEN,NT5DC2,MYEOV,CEP290,ALAS1,MADD,SLC22A8,HMGA1,MCTP1,RPS6KB2,ST8SIA5,DMAP1,CCNG2,DEFB4B,SLC25A20,TMEM184A,SLC26A10,SPACA4,ZNF491,CD37,PRMT5,CYP4F12,IL32,KDSR,CTAG1B,TRMT12,CLEC4G,SLC52A2,ANKRD11,TMEM89,NAT8L,ACSM5,PGP,CCDC84,VSTM2B,FRMD1,ZFYVE19,ESR1,NAPRT,TBC1D16,OAS2,CD55,SLC35E4,CASZ1,PCNX2,SDSL,ZNF683,GPAA1,KEL,OR8B4,XAB2,KCNN3,LFNG,NIF3L1,MAP4,DISP1,FLNA,TEDC2,SCAMP5,GLMP,TPR,LY9,CD1E,SH2D2A,KHDC4,CALHM6,SELENBP1,ACADSB,RPRD2,LDOC1,ZDHHC16,DIRAS3,SLC29A1,RAPGEF1,CD40,YIPF3,TFAP2E,TMEM35B,TGIF2,MFSD14C,SP5,WDR45,SPATA31A7,BTN3A2,PCDHA4,SEPT8,DCTN3,TTLL10,AVP,SLC22A23,ARHGAP6,MTUS2,SLC13A5,ITSN1,TOM1,ZG16B,CTBP1,ARNTL,KIF19,SIGLEC6,AKT1S1,FCRL6,SORBS2,ANKRD39,SEMA5B,VKORC1,IZUMO4,WDR6,AKAP10,CCDC51,KIR2DL4,DDR1,RAB2A,CHMP1A,TREH,GSTP1,MS4A18,ANO7,NAGA,C2orf73,RHBDD3,RPS14,PIGQ,KCNC4,ADPRHL1,CACNA1B,CHN1,STK11IP,SLC2A6,KIAA0930,A1CF,PGC,FAM229A,IFRD2,SLC2A8,CD6,THNSL2,IFT172,C3orf18,MRPL10,HYAL2,KBTBD2,PSPH,BCS1L,PLA2G6,PHF1,SLCO2B1,PIGV,SENP2,ARHGEF33,SRPK3,ZNF485,RLN3,VAMP8,CLCN1,RNF144A,PSMD2,PFKP,COL6A3,HJURP,SLC12A9,EDEM1,EPM2A,HAUS7,TRIM26,NCDN,SNRK,TST,ZNF382,FBXO34,PDE2A,C16orf91,SEMA3E,FAM90A1,FOLR3,GTF2I,OPN4,OR10C1,CCDC188,BCAS4,GSDME,CCT3,NR5A2,MRPL28,ZNF185,TTC22,ORC5,MBOAT7,TMEM150A,ANAPC1,C2orf92,DOT1L,RBKS,NDUFS8,FAM126B,CLCN4,FOLR2,PDE3B,DCAF6,NELFA,PCSK5,SCMH1,GOLGA2,IRF1,XPNPEP1,KLHDC8A,ATP11C,CFLAR,PPP2R5D,TNNC1,C1orf116,TFPI2,SLC25A48,CBS,PPP1R16B,ALAS2,D2HGDH,ASCC2,MRPS5,PRKD3,PGAP2,IL1RAP,DEGS1,RABL6,PYCR2,GPR157,PLP1,SYP,CYP21A2,MFNG,TMEM8A,PIM3,ARMCX3,CREB3L2,DESI1,INPP4A,TRAIP,SLC35E1,LAS1L,MTA1,OSBPL10,STK36,HKDC1,CKS1B,DPH2,NOM1,RASSF4,PKD1,ACADM,ARF1,NFKBIL1,CNN3,ALPP,DNAL4,TBC1D10B,MFSD4A,UB

 doi:10.20944/preprints202404.0003.v1

	R4,LAMB1,SPINK5,SACS,CLIC5,AP5Z1,FANCC,ITGB3BP,PQLC1,BCR,SETD5,TM9SF4,KREMEN1,SLC38A5,ZC3H11A,CCM2,PDZD4,KDM4A,XKR8,DTNB,PABPC1L,TP53BP2,EWSR1,RGR,COPS6,PDLIM4,STIMATE,NPDC1,CCZ1B,NEBL,TSPAN32,GSDMB,ANKS6,ALB,LBR,ISM2,AC114490.2,ARIH2,RAB11FIP3,PSD,MMP11,TMCO4,MZT2A,CREM,IARS2,UBAC1,CACUL1,ATRAID,TOP2B,C3orf58,ZNF789,AL080251.1,SLC4A2,EIF3B,JAK1,MFSD2B,SH3BP1,AMT,PCMT1,LY6G6C,KDM4C,LAMC1,NRXN2,STX1A,LZTR1,MAST2,TNIP2,DGKQ,MARCH6,ABCC3,NR1I3,ATP13A2,C5orf34,ZDHHC11,INPP4B,PXYLP1,TLR1,SIL1,THAP9,SLC9B2,CHIT1,AMN1,ARL10,RGS7BP,IRF2,IFT122,SDHA,HK3,TRIP13,SPAG9,ZNF451,NADK2,SH3BP2,CEP72,GYPB,WDR36,PCDH1,ZFAND1,TBC1D9B,ATP6V1C1,PIEZO1,RRNAD1,NSMAF,TRIQK,TSPAN18,STC2,ENTPD4,MROH5,ATP6V1H,MTSS1,PRSS55,ERICH1,PHYHIP,REEP4,AARD,DIS3L,ABCA7,PPP6R3,KCNK7,USP47,NUP214,RPS3,C11orf16,ME3,ST5,PACS1,TK2,PRDM10,RIC8A,ARMS2,SULF1,ANO1,TPP1,CDKL1,CTBP2,INTS11,TP53I11,PCNX3,IGLL5,MOB2,MAJIN,CAMSAP2,RCE1,ACAT1,PPP1R16A,TKFC,POLR2L,NUMA1,PTPRO,PLEKHB1,ARAP1,ACSF3,RELT,PDE1B,NCAPD2,IGHMBP2,SLC22A1,FAAP100,MMP20,M6PR,WDR74,DNAH10,MGP,SLC39A3,SUOX,DDI2,TPH2,HECTD4,HVCN1,KRT78,NTN4,GAS2L3,PFKM,CSAD,DUSP6,PLXNC1,DAZAP2,KRT6A,CA6,DDX23,TSPAN8,FICD,ESPL1,HECTD1,ACTN1,PSEN1,ASB2,PCNX1,MIPOL1,SIPA1L1,PPP1R13B,NIPA1,IDH3A,GATM,MAN2A2,EIF5,RNF31,GABPB1,ADCY4,TLN2,GCNT3,DNAJC17,ALDH1A2,PBX4,GMPR2,SEMA4B,CEP152,FAH,SLC9A5,ATXN2L,PLA2G4F,PRMT7,GALNS,CASKIN1,AC090360.1,EXOC3L1,AMFR,CLCN7,CCDC33,ARMC5,C16orf58,NOL3,CNOT1,TAF1C,ZNF688,VAC14,BAIAP3,DDX19B,NLRP1,NEIL1,ABCC11,GEMIN4,SLC25A11,PELP1,CIC,SPACA6,FN3KRP,TSR1,CLUH,FAM57A,CHRNB1,SGSM2,STRA6,CORO7,AKAP1,HCFC1R1,WNT9B,URI1,NAA60,RASSF5,DUS1L,SMARCD2,TTC39C,MYO15B,ADCYAP1,NARF,TMEM94,ITGB4,RAB31,GDPD1,LRRC45,OGFOD3,CDC6,CCDC57,FLOT2,GHDC,WDR7,TEN1,MAU2,HAUS5,ZNF793,MAP3K14,RBFA,HIGD1B,CXXC1,GPATCH8,FHOD3,ROGDI,TMEM161A,ATP9B,EFTUD2,ACTN4,ZNF532,EIF3G,ALPK2,ZACN,LIG3,EPS8L1,NAGLU,SLC7A10,JSRP1,CTAG1A,ARHGEF1,ADGRE2,ECH1,CD22,ILVBL,MCOLN1,HPN,CCDC97,ZNF17,F2RL3,TMEM38A,PPFIA4,EMG1,KCNN4,LIPE,VAV1,FSD1,HNRNPL,SIGLEC7,ZCCHC18,LCE1C,ARFRP1,GRM4,AL034430.1,MYO19,UNC93B1,PCGF2,MED26,TTLL13P,SPPL2B,AC008162.2,SIK1B
hsa-miR-103a-3p	CAMKK1,CNFN,CD69,MXI1,APC,GNB5,TCIRG1,EXPH5,KCTD7,SEC16A,KCNMA1,PKNOX1,TNFSF12,FASTK,HRASLS5,MAP2K1,FAM53A,NOSTRIN,GPR137C,ZAR1,APP,ZFYVE26,MYO9A,SMOC1,SOX13,CFAP46,TTF2,ZNFX1,GLO1,MAP3K8,REL,CYP1A1,TSPAN4,GATD1,NONO,KMT2B,IFT22,MFSD13A,MED20,DGCR6,ZNF879,AL139260.3,DLG2,TMEM72,BRDT,STAT3,PPP1R2,LAMB2,TMEM54,SNX17,MFN1,SLC11A1,ASB18,HECW1,CERCAM,SMARCD3,NDUFV2,DENND2A,TOGARAM2,PLIN2,MMACHC,MRPL38,RNF146,SPTLC1,GTF2IRD2,MPP3,CAPN10,ITGB1BP2,CFP,PTP4A2,TTLL3,SLC2A11,FAM45A,SUB1,MGAT1,ZNF346,CNGA1,FER,ELMOD2,CORIN,WDR17,MZB1,ARL15,UBE2Z,ZNF706,ITK,ACAT1,DDX25,CAPN5,GDPD5,DEAF1,TRMT9B,MRPL16,FKBP4,MLXIP,ARAP1,SLC38A10,LETMD1,ACTR6,ATAD2,DAAM1,TMCO5A,

 doi:10.20944/preprints202404.0003.v1

	DET1,IVD,RPS27L,KATNBL1,MAN2A2,SQOR,METTL22,STX1B,GINS3,SPG7,CDH3,WDR59,PPP1R27,MPDU1,MYCBPAP,ZZEF1,CCNE1,TMEM105,LASP1,CCDC57,ERBB2,CLPTM1,FOSB,KDSR,GPI,DNAJC7,KEAP1,KDM4B,ZFR2,CACNA1A,DAPK3,SIPA1L3,LIG1,ZNF17,IRF3,SNRPA,SELENOW,USP29,EMC8,ELAC2,MMRN2
hsa-miR-122-5p	PPP2R5B,GATC,VPS53,SLC25A34,XPO6,SWI5,NUDT1,GPRC5C,OR2AK2,BGLAP,TSPAN2,BPIFB3,CFAP74,RAB3IP,CAP2,DENND1A,DOT1L,FAM118A,HECW2,G6PC2,VTCN1,FHIT,SLC11A1,THADA,RAC1,CMTR1,STX7,ZP3,SFXN3,PPP2R2D,INPP5K,ZAP70,DMXL1,ETF1,SLC2A9,FUT10,GEMIN5,PLEKHA7,C11orf49,MROH1,FPGT-TNNI3K,GNS,APPL2,UBAP1L,FANCA,BEAN1,SIRT7,RAB8A,DNMT1,CCDC155,NUMBL,TMEM185A
hsa-miR-125b-2-3p	GUCA1A,PTBP3,ISL1,NPC2,SLC52A1,EDAR,HINT2,MUL1,GCKR,SPIB,AWAT2,RPP30,PLEKHG4B,BTG2,SOX8,KCNT2,CAPN13,PF4,CCDC174,B4GALT2,CCPG1,BANF1,TPRX1,WDR45,RPAIN,HCAR2,BRCC3,RTN4RL2,AGAP3,SH2D6,ZKSCAN7,NPAS3,CHRD,THSD4,TBX19,NR1I3,SARDH,MMRN2,KLF17,CLCN5,CYP1A1,CIITA,CHD2,DOK5,NRL,IL25,ARID1B,C19orf24,CD8A,VDAC2,CFAP65,TMEM250,IL1R1,AC037459.1,DPCD,PRSS45,WDCP,AC023509.3,TPR,ZNF674,GLP2R,KCP,ST3GAL5,MICAL3,MRPS31,TRANK1,LAMA5,ABCA2,TFIP11,GTF2I,C2orf42,LETM1,NOL8,PCOLCE,DLG5,ACSS2,ECE1,RNF182,CERCAM,VTI1A,NIT1,ECE2,KRBOX4,SKIL,PPP2R1A,IL11RA,C21orf2,C2orf70,ECHDC2,SPINK5,ROR1,DNER,HLADOA,LRP1B,TMLHE,RGS3,TAB1,IL9R,FAAH,CCT3,ZNF491,LY75,CENPL,PCOLCE2,PER3,MIA3,DGCR8,SSR3,CNIH3,AURKAIP1,GLB1,RPL9,ACAD9,APBB3,TSC22D3,RCHY1,FAM81B,CANX,RNF175,POLR2B,PALLD,CNOT8,CARD8,SPIDR,ZFHX4,ZNF706,ZNF395,MYOZ3,DECR1,CEP57L1,THAP8,IFITM1,PLEKHA7,MTA2,ZNF692,LRP5,HCAR3,C11orf88,SLC37A4,REPS1,SMPD1,C12orf60,NPEPPS,CRACR2B,ATG16L2,ACACB,TM7SF3,C2CD5,MED21,TARSL2,CCDC91,MPHOSPH9,CD163L1,IBA57,CAPS2,ACVRL1,TWF1,MED13L,MAPKAPK5,TNS2,HDAC4,KRT86,LIN52,NAB2,EAPP,PAK6,TIPIN,CDH11,CARHSP1,UBR1,NRG4,AC026464.3,MYO9A,EARS2,IL4R,ATXN2L,FAN1,CPEB1,ANKFY1,P2RX1,TMEM100,RPL23,PPIAL4A,ASPSCR1,PPIAL4F,PPIAL4E,AC243756.1,PPIAL4C,ZNF559,MOB3A,NKIRAS2,TNNI3,HDHD2,GLYR1,EFTUD2,C18orf25,LIN37,KLK2,LTBP4,ZNF749,PEG3,PHLDB3,ZNF772,AC012254.2,DUSP22
hsa-miR-125b-5p	CYP26B1,MLF2,UBOX5,BCKDK,ANAPC15,PXN,DOK1,ARHGAP40,PACSIN1,LRFN3,MAP3K10,USP29,KMT5C,DDB2,TIMM10,AKAP2,HHAT,OSBPL5,MUL1,ANK2,SFRP5,GFOD2,LRRC46,ZNF593,PTGES2,FAM160B2,CRYAA,FAM207A,IKZF3,MAPKAPK2,ANKRA2,ANPEP,TSC22D4,VPS37C,UTF1,MAP3K11,ABLIM3,MATK,SPEG,BTBD9,CDPF1,AMBRA1,ASB2,CSH1,TMEM107,GADD45GIP1,EIF4E1B,TMEM184A,EHD1,ZNF7,LMNB2,IFNLR1,CTAG1B,HDDC3,SNAI3,SIGIRR,ZNF555,TMLHE,SELENOV,GGT7,OPRL1,ZNF385A,CRTC1,SECISBP2,SP100,SLC26A9,HIST1H2AD,VCX,WDR31,COL11A2,COL18A1,NUTM2B,EPB41,LRRC69,PSMD13,NUTM2G,NEIL1,ADAM11,SERPIN

 doi:10.20944/preprints202404.0003.v1

	H1,EPHA2,ZNF707,SSU72,SIRT5,NT5C1B,BAK1,R3HDM4,SMG5,S100A3,CTAG2,STMN3,DNLZ,AIF1L,GDAP1L1,MANBAL,HSPG2,PLA2G5,SKIV2L,PROSER2,NUTM2D,NUTM2A,RPUSD3,WIZ,PTOV1,CSH2,MED20,UBE2D3,ANKRD13B,CENPO,EMP1,CCDC125,TAGLN2,OTOG,HMX1,CCDC134,UBE2I,COMT,HIC2,TTC7A,VWA3B,MAGEA2B,AFF3,RBM44,MTHFR,DENND6B,MUM1,MECP2,RPS28,SLC19A1,ANLN,SERPINE3,ZNF839,RFC5,POR,CTU1,ADORA2A,C20orf173,DBNL,NUTM2E,AKR1D1,ENTPD6,ZNF780B,HLAF,TOP3B,RGSL1,CRP,EXO1,PNCK,RARRES3,ENO2,FZR1,SPAAR,OSBP2,TMEM131L,MED22,NEK6,AC037459.1,SMARCD2,ADAM12,FANCG,ASCC2,OGFR,C8orf58,SEMA4F,ANKRD60,LYRM4,CFAP65,TBC1D2B,HM13,MGST3,CPT1B,UROD,PDGFRA,DUSP18,PRR14L,SGSM3,C1orf61,RNF103,MIB2,SEMA4D,WDR27,CLSTN1,MPZL1,ACAA1,COL11A1,MOV10,GP6,SSR2,COL21A1,ST7L,SFI1,FGFR2,PARVG,EXOC4,TMPRSS2,NOC2L,TTN,SLC4A11,TSC2,PTPRE,TEP1,PARD3B,ARPC1A,P4HTM,TM2D1,DNAJC11,AUP1,STK11IP,DHX30,TLE6,SNTG2,PARP3,CEP250,LCK,SLCO2A1,ARR3,ARHGEF3,MFAP2,SYNGAP1,PLCD1,NEU1,FES,SEPT8,ABLIM1,QARS,EPS8L3,GPRC5C,ZAP70,PCNX2,NDUFA3,ACP1,LRRC29,RHBDF1,PTPN14,TBC1D5,MUSTN1,PHF1,NR1H3,DNAH1,TCTA,HES2,INTS11,C7orf50,PCYT1A,PIGL,ZBTB48,MDC1,CNBD2,AURKAIP1,ASB3,PTPN18,REG3A,CYB561D2,IKBKG,AGRN,PTK7,NCOR2,MAGEA8,PSAP,CLCNKA,TPI1,ACTR8,HDAC4,SLC2A4RG,HHATL,DNAH10,ADAM10,REG3G,HDAC11,ZC3H12D,CEBPA,P2RX4,FLT4,F12,CDK10,WDR41,PRELID2,COL4A5,PIGG,LYRM9,PDK2,FRMD1,IDUA,ALG1L2,SLC52A1,HARS2,CHCHD6,TRIO,RMDN1,STMN4,GLI4,LYPLA1,ADAM18,AP3M2,DECR1,RAB11FIP1,PNMA2,RPS6KA1,SIGLEC10,FHAD1,MCAM,TP53I11,SPAG11A,GSDMD,PTPRU,TMPRSS13,TTC12,PRMT1,ZNF250,CHID1,ZDHHC5,SPAG11B,GATD1,BRMS1,ST14,DPF2,NDUFS8,SIDT2,E2F8,GRK2,ST5,PLEKHA7,GRAMD1B,SART1,DPP3,OLFML1,TMEM258,TMEM134,MPHOSPH9,CD6,SLC6A12,SFSWAP,VWF,VTN,HIP1R,MMAB,PGA4,PGA5,C1RL,MACROD1,ST8SIA1,PAH,PAX8,IFI27L1,SLC25A29,ITGA7,IDH3A,CCDC33,CD79B,ZNF710,DPP8,PHGR1,CMIP,RSRP1,PRSS36,SPIRE2,CASKIN1,MVP,CDH11,KDM8,RBL2,RPAP1,KIF22,EME2,VAC14,CLEC18A,BRICD5,KATNB1,PLEKHG4,ABCC11,IL34,SLC25A10,CNTROB,SPACA6,AC139530.2,ITGAE,DVL2,CHRNB1,SGSM2,TXNDC17,MRM3,NPLOC4,SLC46A1,ARHGAP44,MAP3K3,RBFOX3,MARCH10,ICAM2,RAB11FIP4,CENPV,RPL36,TBC1D29,TNS4,SCN4A,RAC3,VAPA,GHDC,CATSPERG,SPPL2B,STK11,TMEM161A,DOCK6,CARM1,CXXC1,C19orf66,MAP4K1,PRKAR1A,PODNL1,VMP1,CIRBP,ADAMTSL5,POLRMT,FIZ1,ZNF234,ACP5,APOC4,EPS8L1,C19orf12,COQ8B,PET100,C19orf44,AXL,KLK8,GPR108,FCHO1,ZNF414,SPTBN4,ANGPTL4,SNRPA,SIGLEC7,KXD1,NMRK2,KHSRP,CTAG1A,CD37,SLC25A42,ZNF329,NAPA,TP73,AC116565.1,SSTR3,YTHDF3,HTR2A
hsa-miR-1271-5p	ADCK2,GNA11,HDAC7,AQP2,CBX6,TRIB3,ZMYND10,IL17C,PDCD2L,SDF2L1,EEFSEC,ESPL1,BCO1,FAF2,GIPR,DBH,BUD23,ERBB3,GPR17,AIG1,EML3,SLC24A2,TYSND1,GOLGA6A,FASTK,C9orf24,PACSIN3,PLK1,NLRP4,C2orf54,ASPHD1,GPR137,CLASP2,TEX44,FUT7,CABP1,ZNF771,RPS15A,NLRC3,OR8B8,MCF2L2,MT1E,ID2,FAM129C,BET1L,MT1B,DOK7,CDK11B,ING4,RPS21,SDSL,ATG16L1,MAGED2,GIT2,ENTPD6,MYH7,CDK11A,ITIH2,GOLGA8A,CDC42SE2,ODF2,SLC29A3,SKIV2L,MGME1,PRDM16

 doi:10.20944/preprints202404.0003.v1

	,AC026461.4,CPXM1,GREB1,GPRC5C,BBS1,CELF6,MIEF2,CEP250,RGPD2,SAMD12,SPATA13,CRIP1,RGPD1,THRB,CARF,IFI35,MX2,C21orf33,TVP23C,PROC,POLR1C,SHANK2,SPHK2,EFHD1,OXSM,IFRD1,CARD10,MBD3,C11orf68,CBX5,DBNL,HNF4A,FAM160B2,PLA2G6,CABLES2,F8,FAM171A1,GRAMD4,COL21A1,MBOAT2,SLC12A8,GRAMD1C,TSTD1,CHRNA4,MT1HL1,MIB2,FDPS,WDR31,RAPGEF4,ANO10,ADORA2A,PLXNA3,THADA,CRELD1,IL17D,KIAA2012,HPCA,PRKCZ,LAMB1,SACM1L,P2RY11,RIPOR2,DENND2D,ABCF2,RNF220,RAB34,ERGIC3,ASAP3,RUNDC3B,UTP6,PRPSAP2,GUSB,USP19,EPHA2,TIE1,LAMB2,GBP5,STARD3,AGPAT3,GKN2,MGMT,TBRG4,CUL3,MEGF11,EVA1C,CSTL1,KCNIP3,SREBF1,IFRD2,DRG1,ATP13A1,TTC22,CSF3R,DRC3,SHISA5,ANKRD16,TPRG1,SRC,HDAC6,DMAP1,AZIN2,PLP1,LRRC2,LAMA5,C1orf109,MBP,IQGAP2,PCDH1,KIF13A,ANKHD1,PPAT,HSD17B11,SPATA20,NGFR,MXD3,RNF44,QRFPR,FAM200B,METAP1,ARAP3,PAPSS1,ANXA6,OSR2,GRIA1,FAM83A,SLC39A14,TAF2,ENO3,ARFGAP2,GOLGA8G,CTTN,TMEM262,PIDD1,TPP1,GOLGA8F,PPP1R16A,MMP7,IMMP1L,CDKL1,CREB3L1,PEX5,IPO8,CARS2,NLRC5,CCND1,PRH1,LHX6,SPECC1L,MAP1S,ANO2,OLR1,PACS2,TPCN1,GNPTAB,AL928654.3,CNR1,PRKCH,PTGDR,TTLL5,SLC35F4,MTHFD1,ALDH6A1,TVP23CCDRT4,GLDN,SLC12A1,TM2D3,IGDCC3,NIPA1,MTFMT,SQOR,FAM214A,MT3,GOLGA8S,ATXN2L,GOLGA8M,GRAMD2A,AC090527.2,MAP1LC3B,ADCY7,GOLGA8H,GTF3C1,GGA2,GOLGA8J,GOLGA8T,DDX19B,MAN2C1,VPS53,TVP23B,SLC43A2,SIRT7,RNF213,CFAP52,CYB561,TMEM241,TOP2A,ARHGAP44,MKS1,SAP30BP,WIPF2,BAHCC1,LSM7,AES,ARHGAP33,GIPC1,G6PC,USP32,CDC37,MBD1,CIRBP,AC092073.1,GHDC,GTPBP3,ZNF665,TIMM50,HNRNPM,F2RL3,DLL3,KLK2,PNPLA6,DUSP22,CCL15CCL14,NTMT1,MLLT6,SRCIN1,CCL23,CCL15,PTPRQ
hsa-miR-130b-3p	PRTN3,BCL2L14,TCEA2,PPA2,MRPL37,CNIH4,STXBP5,IPPK,OR10A4,ATP6V0A1,OR10W1,THOP1,AGAP1,WDR43,TRIM2,ADGRG3,AOX1,ANKS6,CXorf65,DLG5,ACSL6,USP37,EXOSC7,ATG2B,PRKD1,USP34,ABL2,LYRM2,FNTA,MTMR9,MYRF,FKBP4,RAB5C,KCNH3,RPS29,APH1B,CNOT1,AKT2,AC099811.2,NDUFA7,C3,INSR,TIMM50,AC010323.1,MFSD14C
hsa-miR-133a-3p	ITGA3,B4GALT7,NGFR,TRO,TRAM2,CDC34,MORC2,NME4,POP4,FBL,SIPA1L3,AEBP1,CDX1,INO80B,DLGAP3,PDZD11,KLRK1,MRPS2,SEC61A1,PYCARD,PIN1,FXR2,CNN1,PRDM12,YIPF2,NAPSA,PPP1R1B,FADS2,TTBK1,CACNG4,GGT5,PPP1R12C,KCNT1,COL5A3,CHFR,SCAMP2,ARHGDIA,SLC47A1,SEC22C,ADAMTSL1,SOGA1,SPARCL1,OSCAR,OBSL1,PDXK,NAGS,FCGR3B,TRIM17,COL6A3,CLEC3B,SENP2,CLEC1B,PRRT2,SLC50A1,KCTD19,DDIT4,SSH3,CLDN15,DNAI2,GABRB3,MMP14,RPL7A,STOML1,RORC,MARCH8,SF3B2,PDZD3,FOXJ1,FOXL2,FAM187A,CMTM1,NELFA,SERPINA11,NCKAP5L,MMP25,MXD4,ZNF385A,FBXL19,BRAT1,TRIP12,TRADD,DHX30,NPHS1,IL27,FGF17,LAT2,PIK3CD,SREBF2,PNMA5,MRPL55,ENAH,FCGR3A,PFDN2,DNASE1L1,EDN3,SLC2A6,PREX1,LRRC73,FAM167B,KIF12,MSANTD3,MGAT5B,STK19,RSG1,MPIG6B,DLG2,ACTN1,CNNM4,PLXDC2,ACSF3,SHROOM1,NUDT2,CDKN2A,FUS,C1QTNF7,LNP1,IL17RE,ABL1,PTTG1,KCNK7,CELF6,FGFR1,GSTP1,COL13A1,MYL5,ARVCF,DPP6,ABLIM2,CCDC103,SLC35G6,ATP5MFPTCD1,PSMB9,C2orf76,TRAF2,DDAH2,GRPEL2,RASAL1,EPCAM,SFXN4,CD22,CERCAM,BRPF1,OGFOD2,CEP25

 doi:10.20944/preprints202404.0003.v1

	0,TTC38,FAM182B,GIGYF2,SDCBP,PRDM1,PICK1,MRPS18A,RPL10,MGAT1,TULP1,LSP1,KCTD15,PIGV,RLN3,MICAL1,PILRA,MLPH,SERPINE2,POLD2,NCOA6,SH3BP2,MMP23B,EMID1,SEC14L2,GCK,PCED1A,FAM20B,TSSC4,LCP1,ELF3,CCT3,ZNF185,PILRB,TTC31,ASCC2,RASA4,ACAP2,SMIM34A,FCAMR,DMKN,ACTR1B,RHBG,GSS,COL9A3,TGM2,PLEKHA3,BACH2,KLC4,ARFGAP3,PLA2G6,TTLL6,CLCN2,PFKL,DXO,ZNF862,STK40,KEL,NADK,MAMDC2,SCAMP4,SHANK1,APP,MRPS5,ABCA2,PEX5L,NDUFB8,TFDP2,CCDC13,LANCL2,RHBDD2,RNF13,PSORS1C1,MSH5,SNORC,CYP2J2,SURF6,B9D1,FAAH,CRAMP1,SH2D3C,WDR54,CXorf56,HSPH1,EFNA3,MYO1A,KLHDC8B,IL1RN,ACAP3,TBC1D2B,MXRA8,AL096711.2,SSBP1,RRAGB,SPAG8,CPA1,FAM129B,HMGCS2,NRP2,DNASE1L3,PDZRN3,NFKBIE,CACNA2D3,MAGED4,BCAR3,WHRN,MAGED4B,EXOSC7,IZUMO4,ZNF783,NT5C3B,CNTN2,AC093668.2,YPEL5,MLF1,ZNF391,PDS5B,EZH2,PKN3,POLR3H,TAF1,COG5,OPHN1,CLASP1,MYCBPAP,ZNHIT1,PPIL2,PRSS53,PRKCB,CDS2,TRIM56,FUBP3,CCDC150,NISCH,NGEF,DDC,PRRC2B,PNPLA7,RREB1,CBS,DOPEY2,ARPC1B,NCOR2,RABL2A,NICN1,DEPDC5,TSC22D1,LRP8,OGDHL,GYG1,UBE2G2,HM13,ARHGAP8,CEBPA,SH3RF1,PGM3,MZB1,TRIML2,PITX1,NFKB1,KLHL3,HK3,ACAD9,SEC24D,FAM193B,IPO11,FGFRL1,SLC10A7,SRPK1,MGAT4D,EXOC3,AXDND1,CFI,CORIN,COL12A1,ANKHD1,ATP8A1,NR1I3,ABHD18,BFSP2,LMAN2,CPLX2,ACOX3,ZNF704,NDRG1,VIRMA,TMPRSS4,AC105052.1,SNX31,GRIA1,MGAT4B,SORBS3,VDAC3,SLC39A14,ST3GAL1,TRIQK,NKX63,TBC1D9B,PITPNM1,CCDC17,C1QTNF5,ZNF250,TESPA1,ZNF195,PPP2R5B,PPP1R16A,NKAPD1,CHMP4A,TYK2,BACE1,ARHGEF4,ECE1,ZNHIT2,LRP5,AMPD2,TMEM86A,SART1,CKLFCMTM1,EFEMP2,MRPL17,SMPD1,NDUFS8,BBOX1,DNHD1,STK33,PCSK7,ATM,SIPA1,P2RX3,TPCN2,GPR162,KIAA1551,PDE2A,RHOF,CARS2,SRGAP1,SLC6A12,TRMT10B,EHD2,VWF,STAT6,IDH2,NDUFA9,RASA4B,NOP2,MEIS1,KLRC4KLRK1,PLEKHB1,WSCD2,ZNF606,MAP1LC3B2,MCRS1,MARCH9,EEA1,SOCS2,FKBP11,GATC,ARHGAP9,TNS2,ITGA5,ITGA7,SDR39U1,SLC7A7,WDR25,CD63,AKT1,RPS6KL1,CRTC3,TPM1,GCNT3,RTF1,SLC22A31,TK2,MYO7B,KCTD13,KLHDC4,CBFA2T3,NEIL1,CDH16,CEMP1,CMIP,ABCA3,DHX38,NTHL1,LMF1,SMPD3,VPS35L,STARD13,SLC38A8,LDHD,TCF4,ADCY7,ZSCAN29,MAPK7,AKAP10,PLD2,ATP2A3,ZP2,RPS15A,SLC26A11,AKAP1,PELP1,ALDH3A1,DPH1,POLR2A,NXN,PER1,RAB11FIP4,ITGB4,LLGL2,PIEZO2,SUPT4H1,PROCA1,SLC25A35,SEPT4,ARL5C,SLC16A3,EIF4A1,PRR29,ERBB2,PRKCA,TSEN54,CD300LF,MTMR4,CDK12,RPL26,TMEM94,MUM1,PCSK4,UBXN6,MATK,TLE2,EDDM13,NAT14,NEDD4L,PALM,BCAM,APLP1,POLRMT,ATP5F1D,AP1M1,RFX2,SPHK2,SH3GL1,SNAPC2,NAPA,PGPEP1,ETHE1,MYDGF,IRF3,KCNN4,MRPL34,SLC17A7,ARHGEF1,VAV1,PPFIA4,PPFIA3,MORN1,TBX18,CCL15-CCL14,DGKK,AC239799.1,CTDP1
hsa-miR-184	ANKRD54,PEX11G,SF1,MTUS2,AMPD2,TMEM184A,NLGN2,ZBTB46,C20orf196,TCTN2,ATP13A2,CARM1,CACNA1G,TOMM20L,TRIM27,KLF6,TSSC4,PPP1R21,AURKA,MTA1,HMCN2,PTRH1,RLN3,MAP6,CLUH,METTL8,PABPC4,AXIN1,HM13,SLC26A9,PHF21B,TLE1,ABCA2,CDC25B,DPYSL4,FAM83F,S100PBP,SLC2A4RG,ST6GALNAC4,AKT2,TRDMT1,MTMR11,KRTDAP,TARS2,GAL3ST4,ARHGEF10L,CTSA,PHF24,CTSZ,ARHGEF7,DGCR8,TACC2,IFT22,PPP2R3B,LHFPL4,UGT2A1,CDK18,EXOC1L,EFNA5

 doi:10.20944/preprints202404.0003.v1

	,SPAG9,MGAT4B,STK3,LRRC6,FUT2,STT3A,TMEM80,SIGIRR,UBQLN1,ROBO3,ZSCAN9,C1RL,ARHGEF40,NRDE2,TTC7B,PSMA4,PSME2,CACNA1H,ZKSCAN2,FAM192A,ABAT,RNF167,NXN,ELAC2,CTC1,GPRC5C,PTBP1,AP3D1,PIP5K1C,LTBP4,LGALS4,SIPA1L3,PAFAH1B3,IRGQ,KANTR
hsa-miR-203a-3p	SLC26A10,PRKG1,ACVR1,FTSJ3,FOXK2,CCM2,SIM2,SLC35B1,ITGA1,DDX55,GMFB,SUSD6,FUS,LSM7,APOC1
hsa-miR-206	GTPBP1,LY96,SOCS1,TCF7L2,TCTN3,NOTCH4,TRIM31,BSCL2,ELMOD3,ASCC2,TMEM178A,COL20A1,MRO,ZNF33A,SFTPC,FAM120A,AQP12B,AQP12A,ROBO2,PER3,GSTO2,SLC25A12,OCIAD1,RHOBTB3,ASPH,PDP1,GDPD5,ZC2HC1C,FBRSL1,TRAF3,CD276,FA2H,CTC1,ATP5F1A,SIPA1L3
hsa-miR-335-5p	SGK3
hsa-miR-551a	DVL2,RPL18A,PCDHB6,IFT43,PCDHB8,PCDHB10,NEUROG3,TYMP,TUBGCP2,SLC2A11,COX10,KAT6A,ADAMTSL1,FAM81A,FAM46B,ZFYVE28,ABCF3,GPR182,ANGPTL4,MMP14,TRPM7,C4orf50,TMEM150B,SORCS2,EWSR1,DYNC2H1,SNRPD2,TRPM3,VKORC1,AC008397.2,ANKRD35,ZNF707,C20orf203,CNIH4,RXFP4,CHTOP,CYB5R4,ZNF451,BTBD17,DCTN3,EIF1AX,GMDS,AKAP17A,MPP1,GPT,ATP2A1,SELENOS,ZSWIM8,ITSN1,CENPM,ELF1,PRSS40B,PPT2,POLM,PASK,VILL,RTL10,ANKRD62,CIZ1,CAP1,PBRM1,APOE,NR2E1,MAGEA10,LSG1,ZNF776,GTF2I,LCNL1,TNK2,ADAP1,SULF2,COLEC11,TADA3,GPAT2,SFTPA1,RGPD5,TMEM114,OGT,SNRNP27,MFSD13A,CAV1,AURKA,GNB1L,WDR74,PRODH,SEMA4F,DENND6B,EIF6,ECE1,DDX43,LTC4S,RND3,CLTA,RARRES2,PLCH1,RWDD2B,ZMIZ1,ACAP3,SCAF11,TFR2,MECOM,MATN1,PLCG1,RGS19,HES4,KIF6,HBA2,MX1,AKAP2,MCF2L,PANK4,TSC22D3,RCC1,SLC2A5,LRCH4,HBA1,IFT172,LZTS2,RGPD6,HLAC,KRBA1,RGPD8,SLC22A18,RMND5B,MEF2C,TMEM110MUSTN1,RFC1,DDR1,KIAA1191,BDH2,FAM149A,KCNQ4,CPE,SPON2,SPAG9,SERF1B,RPL26L1,NCOA2,ADAM28,MPP2,KIF13B,SLC39A14,RSF1,DLG2,BCLAF1,CRACR2B,TNKS1BP1,CHID1,AC135050.2,TRIM29,HINFP,EPS8L2,PITPNM2,OGFOD2,C12orf65,DDX11,UBC,VSIG10,P3H3,KDM2B,C12orf57,FAM180B,TIAM2,CRIP2,SPRYD3,KCNH3,NDRG2,KLC1,EAPP,SLC25A29,DGKA,ALDH1A3,ADCY4,PIF1,PHGR1,IGF1R,GLDN,BCKDK,NIP7,SPG7,GPRC5B,APRT,RPUSD1,ITGAL,CTU2,RIPOR1,FAM192A,GSPT1,SGSH,FLYWCH1,CTRL,FUK,CHRNB1,SLC47A1,FN3KRP,NAT9,AMZ2,PSMC5,SLC46A1,PSMD8,ADAMTSL5,CYTH1,SPRED3,CDIP1,ANKRD27,TBXA2R,GIPC1,PRKAR1A,TMEM161A,FAAP24,GADD45B,CPAMD8,ADAMTS10,NFKB2,KLK2,PPFIA4,SYT3,AC003006.1,VAV1,FAM156B,NDOR1,ANKRD20A3

Subsequently, a comprehensive analysis of the biological processes, cellular components, and molecular functions of all the miRNAs was conducted through Gene Ontology (Figure 4C). The data indicated that the majority of the miRNAs were involved in the regulation of vesicle-mediated

 doi:10.20944/preprints202404.0003.v1

transport in the biological process category. In terms of cellular components, most miRNAs were implicated in cell leading edge, cell-substrate junction, focal adhesion, and cell-substrate adherent junction processes. Concerning molecular function, the predominant roles of miRNAs were related to phospholipid binding, GTPase activator activity, actin binding, and GTPase regulator activity.

Further GO analysis of the miRNAs that exhibited significant upregulation in the enhanced exosomes compared to the naïve exosomes revealed enriched biological processes, with the identified miRNAs being predominantly associated with the regulation of GTPase activity. Among the cellular components terms, the majority of the identified miRNAs were involved in the actin cytoskeleton, while in terms of molecular function, GTPase activator activity was the most common category (Figure 4D).

We subsequently performed a KEGG analysis, and the results revealed that miRNAs expressed in both naïve and enhanced exosomes play roles in axon guidance, endocytosis, protein digestion and absorption, and glycosphingolipid biosynthesis (Figure 4E). Specifically, among the upregulated miRNAs in the enhanced exosomes, a significant proportion were associated with axon guidance, glycosphingolipid biosynthesis, the MAPK signaling pathway, and the B-cell receptor signaling pathway (Figure 4F).

4. Discussion

A woman's overall well-being is intricately linked to the health of her ovaries, which are affected by range of conditions, such as cancer, cysts, polycystic ovary syndrome (PCOS), poor ovarian reserve (POR), and premature ovarian insufficiency (POI). These multifaceted conditions are influenced by a combination of genetic and environmental factors [19]. The molecular intricacies governing processes within the ovary, including estrogen synthesis, oocyte maturation, and cumulus functions, are critical for maintaining reproductive health. Recently, exosome-based products have emerged as promising therapeutic agents for various disorders, including ovarian conditions [20]. This study delves into the roles of cargo molecules within exosomes, both in the lumen and on the surface, providing valuable insights into the molecular mechanisms underlying the treatment of ovarian dysfunction. In this study, we produced a new type of exosome termed "enhanced exosomes" using a novel approach involving specific cell culture conditions. The objective of this study was to determine the unique composition of enhanced exosomes compared to that of naïve exosomes, providing a comprehensive profile of miRNAs and proteins.

Through meticulous analysis and the use of tools such as volcano plots, we found significant overexpression of specific proteins and miRNAs in the enhanced exosomes. These findings suggested the potential involvement of these genes in the treatment of ovarian disorders. According to an extensive literature review, specific proteins and miRNAs recognized for their overexpression in these exosomes have demonstrated therapeutic potential across various ovarian disorders. The expression of several proteins, including EFEMP1, HTRA1, PAM, and SDF4, was significantly greater in enhanced exosomes than in the naïve exosomes. Previous studies have confirmed the important role of these compounds in treating ovarian disorders through different pathways.

EFEMP1, an extracellular matrix protein, is crucial for maintaining the structural integrity of the extracellular matrix in the ovaries—a critical factor for follicular development and ovulation. Mutations in EFEMP1 may compromise the ECM, affecting ovarian tissue function. While EFEMP1 has been associated with various carcinomas, its role in ovarian cancer is unclear [21]. Previous studies have indicated that activation of the AKT signaling pathway can aid in treating POI [22]. Compared with that in naïve exosomes, the expression of EFEMP1 in enhanced exosomes was significantly greater, suggesting a potential impact on ovarian tissue functions.

HTRA1, a gene encoding a serine protease that plays a role in apoptosis and tissue remodeling, is implicated in various cellular processes. Dysregulation of HTRA1 may disrupt ovarian tissue homeostasis, potentially contributing to ovarian disorders. Reduced nuclear expression of HtrA1 is linked to a more favorable prognosis in patients with high-grade serous ovarian carcinoma [23]. Additionally, the degradation of X-linked inhibitor of apoptosis protein (XIAP) by HtrA1 plays a role in the cellular response to chemotherapy, suggesting that restoring HtrA1 expression could be a

 doi:10.20944/preprints202404.0003.v1

promising therapeutic approach for treating ovarian cancer [24]. Based on the protein profiling data, the expression of HTRA1 was significantly greater in the enhanced exosomes than in the naïve exosomes, suggesting the potential increase in the therapeutic efficacy of enhanced exosomes for treating ovarian disorders.

Although the direct involvement of the PAM in ovarian disorders has not been fully defined, its connection to neuropeptides suggests a potential influence on reproductive processes, with implications for ovarian function. PAM inhibits ovarian cancer stem cell (CSC) traits and has synergistic effects when combined with CDDP, indicating that PAM is a promising candidate for intraperitoneal chemotherapy. Accumulating evidence has demonstrated the antitumor effect of plasma-activated medium (PAM) in various carcinomas, including ovarian cancer. This finding suggested the potential for increasing antitumor efficacy while minimizing side effects [25]. Compared with that in naïve exosome, the abundance of PAM in enhanced exosomes was significantly greater, as revealed by our proteomics data. This noteworthy increase in PAM expression in enhanced exosomes suggested a potential antitumor effect, highlighting the therapeutic implications of enhanced exosomes.

SDF4, which is responsible for encoding a stromal cell-derived factor, plays a role in protein folding and secretion. Given the critical importance of proper protein folding for the functionality of ovarian proteins, any dysregulation of SDF4 may contribute to ovarian dysfunction [26]. SDF4 exhibits a notable increase in expression in enhanced exosomes comprised to naïve exosomes, indicating a potential effect on the functions of ovarian tissue.

Among the myriad of regulatory molecules, microRNAs (miRNAs) are key modulators of gene expression. In the field of ovarian disorders, the encapsulation of miRNAs in exosomes is a promising strategy for therapeutic intervention. Through miRNA profiling, we observed significant overexpression of several miRNAs in the enhanced exosomes compared to the naïve exosomes. Based on an extensive literature review, we have demonstrated that these overexpressed miRNAs have therapeutic potential for various ovarian disorders.

MiR-1-3p, a microRNA (miRNA), plays a nuanced role in ovarian function and disease, demonstrating both tumor-suppressive and oncogenic properties contingent on the specific context. As a tumor suppressor, miR-1-3p obstructs cell proliferation, migration, and invasion, restricting the expansion of ovarian cancer cells by targeting crucial genes involved in cell cycle progression, such as c-Met and FZD7 [27,28]. Previous studies have indicated the role of miR-1-3p as a tumor suppressor in different cancers through different mechanisms, such as upregulating SFRP1, repressing E2F5 and PFTAIRE protein kinase 1, and modulating BDNF and TrkB [29–32]. Moreover, miR-1-3p increase chemotherapy sensitivity in ovarian cancer cells by targeting genes associated with drug resistance [28]. Notably, Fu et al. observed significant downregulation of miR-1-3p in ovarian cancer tissues compared to normal tissues [33]. The substantial overexpression of miR-1-3p in enhanced exosomes imparts a tumor-suppressive effect, contributing to their heightened therapeutic potential. Additionally, the presence of this miRNA enhances the sensitivity of ovarian cancer cells treated with enhanced exosomes to chemotherapy, a crucial aspect of the treatment for ovarian cancer.

MiR-103a-3p significantly influences ovarian cancer dynamics by suppressing CHI3L1, effectively inhibiting proliferation and angiogenesis. This change strongly inhibits ovarian lymphatic metastasis and distant metastasis, potentially involving the TGF-β pathway [34]. The overexpression of miR-103a-3p in enhanced exosomes exerts a regulatory effect on controlling ovarian cancer.

MiR-122-5p is recognized for its tumor-suppressive functions in various cancers [35–37], and miR-125b-5p, known for its low expression in diverse tumor tissues [38], plays important roles in ovarian cancer. Previous studies have demonstrated that miR-122-5p inhibits the migration, invasion, and metastasis of ovarian cancer cells by targeting the P4HA1 gene [35] and suppressing proapoptotic proteins [39]. Additionally, Chen et al. reported the downregulation of miR-125b-5p in ovarian cancer cells, emphasizing its role in inhibiting migration and invasion [40]. Notably, miR-125b-5p negatively regulates CD147 expression, contributing to the inhibition of ovarian cancer cell migration and invasion. Our miRNA sequencing analysis of the enhanced exosomes and naïve exosomes revealed

 doi:10.20944/preprints202404.0003.v1

significantly greater expression of miR-122-5p in the enhanced exosomes. Given the confirmed role of miR-122-5p as a tumor suppressor that can control the migration and invasion of ovarian cancer cells, enhanced exosomes secretion may be an effective strategy for the treatment of ovarian cancer.

MiR-1271-5p is a cancer suppressor, as demonstrated by Liu et al., and its overexpression is linked to inhibition of ovarian cancer growth through the targeting of CCNG1[41]. Moreover, this miRNA directly targets E2F5, a key player in DNA synthesis, negatively regulating the mTOR signaling pathway and hindering the development of ovarian cancer cells [42]. Additionally, miR-1271-5p directly targets TIAM1, a gene associated with metastasis, leading to the deactivation of the Notch signaling pathway and the consequent inhibition of ovarian cancer progression [42]. MiR-1271-5p was identified as another miRNA that is significantly overexpressed in enhanced exosomes compared to naïve exosomes, as indicated by our miRNA profiling results. Given the cancer suppressor effect and its inhibitory role in cancer progression associated with this miRNA, the enhanced exosome secretion, which is associated with elevated expression of miR-1271-5p, holds therapeutic potential for the treatment of ovarian cancer.

A previous study indicated that miR-133a-3p expression is downregulated in ovarian cancer tissues compared with nontumor tissues. MiR-133a-3p negatively regulates the expression of PYGB by binding to the 3′-UTR of PYGB and ultimately inhibiting ovarian cancer development via the Wnt/B-catenin signaling pathway [43]. In a different study, miR-133a was shown to act as a tumor suppressor and to inhibit the proliferation, differentiation, and motility of cancer cells via different mechanisms, such as targeting several oncogenes, targeting the EGFR/Akt signaling pathway, and inhibiting IGF1R expression [44–47]. MiR-133a plays diverse roles in controlling ovarian cancer through its involvement in various signaling pathways. Moreover, the overexpression of this miRNA in enhanced exosomes, compared to that in naïve exosomes, suggests the potential to increase the therapeutic efficacy of enhanced exosomes in the context of ovarian cancer.

MiR-184 is downregulated in ovarian cancer cells and tissues, and its overexpression induces apoptosis and inhibits cell proliferation [48,49]. The expression of miR-203a-3p is lower in ovarian cancer tissue than in normal tissue. Liu et al. demonstrated that miR-203a-3p is an anti-oncogenic factor in ovarian cancer. Overexpression of this miRNA in ovarian cancer cells inhibits cell proliferation, invasion, and migration; induces apoptosis; and arrests the cell cycle in the G1 phase by targeting ATM. This regulatory mechanism influences the Akt/GSK-3B/Snail signaling pathway, contributing to the control of ovarian cancer proliferation [50]. In a separate study, miR-203a-3p was reported to target CXCL1 at the mRNA level, leading to the inhibition of proliferation, migration/invasion, and angiogenesis in ovarian cancer cells [51]. This finding is attributed to the role of CXCL1, which, when attached to the cell surface receptor CXCR2, activates various pathways, including the PI3K/Akt, PLC/PKC, Ras/Erk, and JAK2/STAT3 signaling pathways [52]. MiR-206 plays a pivotal role in inhibiting ovarian cancer proliferation through diverse mechanisms, as confirmed in several studies. This molecule can directly target c-Met, suppressing the activation of the downstream AKT/mTOR signaling pathway [53]. Alternatively, miR-206 targets KIF2A, leading to the inhibition of cancer cell proliferation, migration, invasion, and induction of apoptosis [54]. Additionally, miR-206 targets CCND1 and CCND2, inhibiting the proliferation, progression, migration and invasion of ovarian cancer cells [55]. In estrogen-dependent tumors, this miRNA targets PFKFB3, regulating cancer cell proliferation through GLUT1, PFKFB3, and FAK [55]. Another study highlighted the anti-growth effect of miR-206 in ovarian cancer and its ability to increase chemotherapy sensitivity by targeting CDK4 [56]. MiR-184, miR-203a-3p, and miR-206, which are downregulated in ovarian cancer, play pivotal roles in controlling cancer cell proliferation, reducing metastasis, and inhibiting invasion through the targeting of various genes and signaling pathways. Notably, the significant overexpression of all three miRNAs in enhanced exosomes suggested a promising therapeutic strategy for ovarian cancer.

With respect to polycystic ovarian syndrome (PCOS), various studies have reported a notable reduction in the expression of miR-103a-3p, miR-106a-5p, and miR-125b-5p in PCOS patients compared to control subjects [57–60]. Changes in the expression of these genes were found to modulate pathways associated with axon guidance, MAPK signaling, endocytosis, circadian

 doi:10.20944/preprints202404.0003.v1

rhythms, and cancer. In PCOS, elevated Pak3 expression inhibits ERK1/2 activation, leading to reduced estradiol production, granulosa cell death, and increased testosterone production. MiR-125b-5p binds to Pak3, reducing its expression. Consequently, activated ERK1/2 induces estradiol production and inhibits granulosa cell death and testosterone production [60].

McAllister et al. conducted a target prediction analysis and found that miR-130b-5p may target PCOS-related genes, including DENND1, ZNF217, RAB5B, LHCGR, ERBB3, and KCNA4 [61]. The study indicated that DENND1A.V2, increased the expression of both CYP17A1 and CYP11A1, which are responsible for androgen production in the theca cells of PCOS patients. MiR-130b-3p was implicated in the translational regulation and expression of DENND1A.V2. Pathway and network analyses suggested that miR-130b-3p inhibits the upregulation of DENND1A and RAB5B, influencing the expression of theca cell LH receptors at the cell surface. Additionally, miR-130b-3p interacts with insulin signaling through the MAP kinase pathway. Notably, forskolin stimulation induced the translocation of DENND1A.V2 and RAB5B to the nucleus, indicating their potential direct stimulation of steroidogenesis [62]. In a separate study, Waterbury et al. investigated the relationship between ZNF217 and miR-130b-3p in PCOS patients. The study revealed that ZNF127 expression is elevated in granulosa cells and theca cells, leading to increased estradiol synthesis in the granulosa cells of healthy women. These findings suggest that ZNF217, indirectly regulated by the intermediary of miR-130b-3p, downregulates the expression of DENND1A.V2 and subsequently the expression of CYP17A1 [63]. Our miRNA profiling analysis revealed significantly greater expression of miR-125b-5p and miR-130b-5p in enhanced exosomes than in naïve exosomes. This findings suggested that enhanced exosomes therapy may have greater therapeutic efficacy than naïve exosomes therapy for polycystic ovary syndrome (PCOS).

Premature ovarian insufficiency (POI) is characterized by the induction of apoptosis in granulosa cells, and is a hallmark of the disease. Lv et al. reported the significant upregulation of miR-130b-3p in association with a negative correlation with PTEN expression. Similarly, miR-130b-3p was found to target and downregulate PTEN, an inhibitor of the PI3K/AKT/mTOR signaling pathway. The inhibition of PTEN by miR-130b-3p led to the activation of this pathway, ultimately suppressing apoptosis and promoting cell survival [64]. Moreover, the study highlighted SMAD as another target gene of miR-130b-3p. Moreover, SMAD plays a crucial role in the proliferation of granulosa cells. Consequently, the overexpression of miR-130b-3p was shown to enhance the viability and proliferation of granulosa cells, revealing the intricate molecular mechanisms contributing to the pathogenesis of POI [65].

5. Conclusions

In conclusion, this study highlights the distinct cargo of enhanced exosomes compared to naïve exosomes, identifying a novel frontier in exosome-based therapy for diverse ovarian disorders. To confirm their enhanced therapeutic potential, researchers should further elucidate the specific mechanisms of action and the responsible molecules guiding their efficacy. This knowledge will lay the foundation for targeted applications of enhanced exosomes, offering a valuable pathway for advancing therapeutic interventions for women's reproductive health.

Supplementary Materials: The following supporting information can be downloaded at the website of this paper posted on Preprints.org. Table S1: Significantly Overexpressed Proteins in Enhanced Exosomes Compared to Naïve Exosomes Across All Categories (All Proteins, Extracellular Vesicle, and Exosome), Including Fold Change Analysis; Table S2: KEGG Pathway Analysis of Proteins Overexpressed in Enhanced Exosomes Compared to Naïve Exosome; Table S3: Complete List of Upregulated and Downregulated miRNA in Enhanced Exosomes Compared to Naïve Exosomes, Including Fold Change and p-Value; Figure S1: The expression of exosomoal markers; Figure S2: Network of Known miRNAs and Their Target Genes.

Author Contributions: Conceptualization, M.M.G, F.L, H.P, and A.A.; Formal Analysis, M.M.G, M.H., A.H., S.H.S.W. and S.V.; Investigation, M.M.G., F.L., H.P., M.H., A.H., and S.H.S.W. ; Project administration, M.M.G; Writing-orginal draft, M.M.G, S.H.S.W., A.H., and S.V.; Writing-review and editing, M.M.G, and A.A. Supervision, A.A; Funding acquisition: A.A. All authors actively participated in reviewing and approving the final manuscript.

Funding: This study was financially supported by start-up funds from the University of Chicago.

Data Availability Statement: The raw data supporting the conclusions of this article will be made available by the authors on request.

Acknowledgments: Electron microscopy was performed at The University of Chicago Advanced Electron Microscopy Core Facility (RRID:SCR_019198). A proteomics study was conducted at the University of Chicago Proteomics Platform (RRID:SCR_022928).

Conflicts of Interest: The authors declare that they have no competing interest.

References

1. Gurung, G.; Perocheau, D.; Touramanidou, L.; Baruteau, J. The exosome journey: from biogenesis to uptake and intracellular signalling. *Cell Commun Signal* **2021**, 19, 47.
2. McNamara, R.P.; Dittmer D.P. Modern Techniques for the Isolation of Extracellular Vesicles and Viruses. *J Neuroimmune Pharmacol* **2020**, 15, 459-472.
3. Zhao, R.; Zhao, T.; He, Z.; Cai, R.; Pang, W. Composition, isolation, identification and function of adipose tissue-derived exosomes. *Adipocyte*, **2021**, 10, 587-604.
4. Colombo, M.; Raposo ,G.; Théry, C. Biogenesis, secretion, and intercellular interactions of exosomes and other extracellular vesicles. *Annu Rev Cell Dev Biol* **2014**, 30, 255-89..
5. Bella, M.A.D. Overview and Update on Extracellular Vesicles: Considerations on Exosomes and Their Application in Modern Medicine. *Biology (Basel)* **2022**, 11, 804.
6. Saad, M.H.; Badierah, R; Redwan, E.M.; El-Fakharany, E. M. A Comprehensive Insight into the Role of Exosomes in Viral Infection: Dual Faces Bearing Different Functions. *Pharmaceutics* **2021**, 13, 1405.
7. Kowalczyk, A.; Wrzecińska, M.; Czerniawska-Piątkowska, E.; Kupczyński, R. Exosomes – Spectacular role in reproduction. *Biomed Pharmacother* **2022**. 148.
8. Baranyai, T.; Herczeh, K.; Onódi, Z.; Voszka, I.; Módos, K.; Marton, N.; Nagy, G.; Mäger, I.; Wood, M.J.; El Andaloussi, S.; Pálinkás, Z.; Kumar, V.; Nagy, P.; Kittel, A.; Buzás, E.I.; Ferdinandy, P.; Giricz, Z. Isolation of Exosomes from Blood Plasma: Qualitative and Quantitative Comparison of Ultracentrifugation and Size Exclusion Chromatography Methods. *PloS One* **2015**, 10.
9. Street, J.M.; Koritzinsky E.H.; Glispie, D.M.; Star, R.A.; Yuen, P.S.T. Urine Exosomes: An Emerging Trove of Biomarkers. Adv Clin Chem **2017**, 78, 103-122.
10. Cheshmi, B.; Cheshomi H. Salivary exosomes: properties, medical applications, and isolation methods. *Mol Biol Rep* **2020**, 47, 6295-6307.
11. Han, J.S.; Kim, S.E.; Jin, J.Q; Park, N.R.; Lee, J.Y.; Kim, H.L.; Lee, S.B.; Yang, S.W.; Lim D.J. Tear-Derived Exosome Proteins Are Increased in Patients with Thyroid Eye Disease. *Int J Mol Sci* **2021**, 22, 1115.
12. Galley, J.D.; Besner, G.E. The Therapeutic Potential of Breast Milk-Derived Extracellular Vesicles. *Nutrients* **2020**, 12, 745.
13. Zamani, P.; Fereydouni, N.; Butler, A.E.; Navashenaq, J.G.; Sahebkar, A. The therapeutic and diagnostic role of exosomes in cardiovascular diseases. *Trends Cardiovasc Med* **2019**, 6, 313-323.
14. Wang, X.; Tian, L.; Lu, J.; Ng, I.O.L. Exosomes and cancer - Diagnostic and prognostic biomarkers and therapeutic vehicle. *Oncogenesis* **2022**, 11, 54.
15. Zhang, H.G.; Grizzle, W.E. Exosomes: a novel pathway of local and distant intercellular communication that facilitates the growth and metastasis of neoplastic lesions. The Am J Pathol **2014**, 184, 28-41.
16. Kar, K.; Dhar, R.; Mukherjee, S.; Nag, S.; Gorai, S.; Mukerjee, N.; Mukherjee, D.; Vatsa, R.; Jadhav, M.C.; Ghosh, A.; Devi, A.; Krishnan, A.; Thorat, N.D. Exosome-Based Smart Drug Delivery Tool for Cancer Theranostics. *ACS Biomater Sci Eng* **2023**, 9, 577-594.
17. Chen, H.; Wang, L.; Zeng, X.; Schwarz, H.; Nanda, H.S.; Peng, X.; Zhou, Y. Exosomes, a New Star for Targeted Delivery. *Front Cell Dev Biol* **2021**, 9.
18. Zeng, H.; Guo, S.; Ren, X.; Wu, Z.; Liu, S.; Yao, X. Current Strategies for Exosome Cargo Loading and Targeting Delivery. *Cells* **2023**, 12, 1416.
19. Kumar, R.; Minerva, S.; Shah, R.; Bhat, A.; Verma, S.; Chander, G.; Bhat, G.R.; Thapa, N.; Bhat, A.; Wakhloo, A.; Ganie, M.A. Role of genetic, environmental, and hormonal factors in the progression of PCOS: A review. *journal of reproductive healthcare and medicine* **2022**, 3.
20. Park, H-S.; Chugh, R.M.; Seok, J.; Cetin, E.; Mohammed, H.; Siblini, H.; Ali, F.L.; Ghasroldasht, M.M.; Alkelani, H.; Elsharoud, A.; Ulin, M.; Esfandyari, S.; Al-Hendy, A. Comparison of the therapeutic effects

 doi:10.20944/preprints202404.0003.v1

between stem cells and exosomes in primary ovarian insufficiency: as promising as cells but different persistency and dosage. *Stem Cell Res Ther* **2023**, 14, 165.

21. Yin, X.; Fang, S.; Wang, M.; Wang, Q.; Fang, R.; Chen, J. EFEMP1 promotes ovarian cancer cell growth, invasion and metastasis via activated the AKT pathway. *Oncotarget* **2016**, 7, 47938-47953.
22. Shi, Y.Q.; Zhu,X.T.; Zhang, S.N.; Ma, Y.F.; Han, Y.H.; Jiang, Y.; Zhang, Y.H. Premature ovarian insufficiency: a review on the role of oxidative stress and the application of antioxidants. *Front Endocrinol* **2023**, 14.
23. Gagné, A,; Têtu, B.; Orain, M.; Turcotte, S.; Plante, M.; Grégoire, J.; Renaud, M-C.; Bairati, I.; Trudel D. HtrA1 expression and the prognosis of high-grade serous ovarian carcinoma: a cohort study using digital analysis. *Diag Pathol* **2018**, 13, 57.
24. He, X.; Khyrana, A.; Maguire, J.L.; Chien, J.; Shridhar, V. HtrA1 sensitizes ovarian cancer cells to cisplatin-induced cytotoxicity by targeting XIAP for degradation. *Int J cancer* **2012**, 130, 1029-35.
25. Lee, Y.J.; Kim, S.W.; Jung, M.H.; Kim, Y.S.; Kim, K.S.; Suh, D.S.; Kim, K.H.; Choi, E.H.; Kim, J.; Kwon, B.S. Plasma-activated medium inhibits cancer stem cell-like properties and exhibits a synergistic effect in combination with cisplatin in ovarian cancer. F*ree Radic Biol Med* **2022** 182, 278-288.
26. Shinozuka, T.; Kanda, M.; Shimizu, D.; Umeda, S.; Takami, H.; Inokawa, Y.; Hattori, N.; Hayashi, M.; Tanaka, C.; Nakayama, G.; Kodera, Y. Identification of stromal cell-derived factor 4 as a liquid biopsy-based diagnostic marker in solid cancers. *Sci Rep* **2023**, 13, 15540.
27. Qu, W.; Chen, X.; Wang, J.; Lv, J.; Yan, D. MicroRNA-1 inhibits ovarian cancer cell proliferation and migration through c-Met pathway. *Clin Chim Acta* **2017**, 473, 237-244.
28. Zhang, D.; Qu B.; Hu, B.; Cao, K.; Shen, H. MiR-1-3p enhances the sensitivity of ovarian cancer cells to ferroptosis by targeting FZD7. *Zhong Nan Da Xue Xue Bao Yi Xue Ban* **2022**, 47, 1512-1521.
29. Shang, A.; Yang, M.; Shen,F.; Wang, J.; Wei, J.; Wang, W.; Lu, W.; Wang, C.; Wang, C. *MiR-1-3p Suppresses the Proliferation, Invasion and Migration of Bladder Cancer Cells by Up-Regulating SFRP1 Expression. Cell Physiol Biochem* **2017**, 41, 1179-1188.
30. Li, S-M.; Wu, H-L.; Yu, X.; Tang, K.; Wang, S-G.; Ye, Z-Q.; Hu, J. The putative tumour suppressor miR-1-3p modulates prostate cancer cell aggressiveness by repressing E2F5 and PFTK1. *J Exp Clin Cancer Res* **2018**, 37, 219.
31. Gao, L.; Yan, P.; Guo, F.F.; Liu, H.J.; Zhao, Z.F. MiR-1-3p inhibits cell proliferation and invasion by regulating BDNF-TrkB signaling pathway in bladder cancer. *Neoplasma* **2018**, 65, 89-96.
32. Dai, S.; Li, F.; Xu, S.; Hu, J.; Gao, L. The important role of miR-1-3p in cancers. *J Transl Med* **2023**, 21, 769.
33. Fu, Y.; Liu, H.; Long, M.; Song, L.; Meng, Z.; Lin, S.; Zhang, Y.; Qin, J. Icariin attenuates the tumor growth by targeting miR-1-3p/TNKS2/Wnt/β-catenin signaling axis in ovarian cancer. *Front Oncol* **2022**, 12.
34. Liften Y,l Wei, S.; Dawei, X.; Jun, W.; Ran, G. Mechanisms of miR-103a-3p/CHI3L1 in proliferation and vascular mimicry of ovarian cancer cells. *J Int Oncol* **2020**.
35. Duan, Y.; Dong, Y.; Dang, R.; Hu, Z.; Yang, Y.; Hu, Y.; Cheng, J. MiR-122 inhibits epithelial mesenchymal transition by regulating P4HA1 in ovarian cancer cells. *Cell Biol Int* **2018**, 42, 1564-1574.
36. Zhang, H.; Xu, S.; Liu, X. MicroRNA profiling of plasma exosomes from patients with ovarian cancer using high-throughput sequencing. *Oncol lett* **2019**, 17, 5601-5607.
37. Huang, X.; Luo, Y.; Li, X. Circ_0072995 Promotes Ovarian Cancer Progression Through Regulating miR-122-5p/SLC1A5 Axis. *Biochem genet* **2022**, 60, 153-172.
38. Li, J.; You, T.; Jing, J. MiR-125b inhibits cell biological progression of Ewing's sarcoma by suppressing the PI3K/Akt signalling pathway. *Cell Prolif* **2014**, 47, 152-60.
39. Sen, A.; Prizant, H.; Light, A.; Biswas, A.; Hayes, E.; Lee, H-J.; Baead, D.; Gleicher. N.; Hammes, S.R. Androgens regulate ovarian follicular development by increasing follicle stimulating hormone receptor and microRNA-125b expression. *Proc Natl Acad Sci U S A* **2014**, 111, 3008-13.
40. Chen, P.; Sun, L-S.; Shen, H-M.; Qu, B. LncRNA KCNQ1OT1 accelerates ovarian cancer progression via miR-125b-5p/CD147 axis. *Pathol Res Pract* **2022**, 239.
41. Liu, X.; Ma, L.; Rao, Q.; Mao, Y.; Xin, Y.; Xu, H.; Li, C.; Wang, X. MiR-1271 Inhibits Ovarian Cancer Growth by Targeting Cyclin G1. *Med Sci Monit* **2015**, 19, 3152-3158.
42. Li, Q.; Shi, J.; Xu, X. MicroRNA-1271-5p inhibits the tumorigenesis of ovarian cancer through targeting E2F5 and negatively regulates the mTOR signaling pathway. *Panminerva Med* **2021**, 63, 336-342.

43. Chiyomaru, T.; Enolida, H.; Tatarano, S.; Kawahara, K.; Uchida, Y.; Nishiyama, K.; Fujimura, L.; Kikkawa, N.; Seki, N.; Nakagawa, M. miR-145 and miR-133a function as tumour suppressors and directly regulate FSCN1 expression in bladder cancer. *Br J Cancer* **2010**, 1-2, 883-91.
44. Kojima, S.; Chiyomaru, T.; Kawakami, K.; Yoshino, H.; Enokida, H.; Nohata, N.; Fuse, M.; Ichikawa, T.; Naya, Y.; Nakagawa, M.; Seki, N. Tumour suppressors miR-1 and miR-133a target the oncogenic function of purine nucleoside phosphorylase (PNP) in prostate cancer. *Br J Cancer* **2012**, 106, 405-13.
45. Cui, W.; Zhang, S.; Shan, C.; Zhou, L.; Zhou, Z. microRNA-133a regulates the cell cycle and proliferation of breast cancer cells by targeting epidermal growth factor receptor through the EGFR/Akt signaling pathway. *FEBS J* **2013**, 280, 3962-74.
46. Guo, J.; Xia, B.; Meng, F.; Lou, G. miR-133a suppresses ovarian cancer cell proliferation by directly targeting insulin-like growth factor 1 receptor. *Tumor Biol* **2014**, 35, 1557-64.
47. Hou, W.; Zhang, Y. Circ_0025033 promotes the progression of ovarian cancer by activating the expression of LSM4 via targeting miR-184. *Pathol Res Pract* **2021, 217.**
48. Qin, C-Z.; Lou, X-Y.; Lv, Q-L.; Cheng, L.; Wu, N-Y.; Hu, L.; Zhou, H-H. MicroRNA-184 acts as a potential diagnostic and prognostic marker in epithelial ovarian cancer and regulates cell proliferation, apoptosis and inflammation. *Phaemazie* **2015**, 70, 668-73.
49. Liu, H-Y.; Zhang, Y-Y.; Zhu, B-L.; Feng, F-Z,.; Zhang, H-T.; Yan, H.; Zhou, B. MiR-203a-3p regulates the biological behaviors of ovarian cancer cells through mediating the Akt/GSK-3β/Snail signaling pathway by targeting ATM. *J Ovarian Res* **2019**, 12, 60.
50. Li, T.; Li, Y.; Rehmani, H.; Guo, J.; Padia, R.; Calbay, O.; Ding, Z.; Jiang, Y.; Jin, L.; Huang, S. Attenuated miR-203b-3p is critical for ovarian cancer progression and aptamer/miR-203b-3p chimera can be explored as a therapeutic. *Advances in Cancer Biology - Metastasis* **2022**.
51. Cheng, Y.; Ma, X-L.; Wei, Y-Q.; Wei, X-W. Potential roles and targeted therapy of the CXCLs/CXCR2 axis in cancer and inflammatory diseases. *Biochim Biophys Acta Rev Cancer* **2019**, 1871, 289-312.
52. Dai, C.; Xie, Y, Zhuang, X.; Yuan, Z. MiR-206 inhibits epithelial ovarian cancer cells growth and invasion via blocking c-Met/AKT/mTOR signaling pathway. *Biomed Pharmacother* **2018**, 104, 763-770.
53. Sheng, N, Xu, Y-Z.; Xi, Q-H.; Jiamg, H-Y.; Wang, C-Y.; Zhang, Y.; Ye, Q. Overexpression of KIF2A is Suppressed by miR-206 and Associated with Poor Prognosis in Ovarian Cancer. *Cell Physiol Biochem* **2018**, 50, 810-822.
54. Chang, L.; Guo, R.; Yuan, Z.; Shi, H.; Zhang, D. LncRNA HOTAIR Regulates CCND1 and CCND2 Expression by Sponging miR-206 in Ovarian Cancer. *Cell Physiol Biochem* **2018**, 49, *Cell Physiol Biochem* **2018**, 49, 1289-1303.
55. Boscaro, C.; Baggio, C.; Carotti, M.; Sandonà, D.; Trevisi, L.; Cignarella, A.; Bolego, C. Targeting of PFKFB3 with miR-206 but not mir-26b inhibits ovarian cancer cell proliferation and migration involving FAK downregulation. *FASEB J* **2022**, 36.
56. Udesen, P.B.; Sørensen, A.E.; Svendsen, R.; Frisk, N.L.S.; Hess, A.L.; Aziz, M.; Wissing, M.L.M.; Englund, A.L.M.; Dalgaard, L.T. Circulating miRNAs in Women with Polycystic Ovary Syndrome: A Longitudinal Cohort Study. *Cells* **2023**, 7.
57. Jiang, X.; Li, J.; Zhang, B.; Hu, J.; Ma, J.; Cui, L.; Chen, Z-J. Differential expression profile of plasma exosomal microRNAs in women with polycystic ovary syndrome. *Fertil Steril* **2021**, 115, 782-792.
58. Qin, Y.; Wang, Y.; Zhao, H.; Yng, Z.; Kang, Y. Aberrant miRNA-mRNA regulatory network in polycystic ovary syndrome is associated with markers of insulin sensitivity and inflammation. *AnnTransl Med* **2021**, 9, 1405.
59. Zhang, X.; Xiao, H.; Zhang, X.; E, Q.; Gong, X.; Li , T.; Han, Y.; Ying, X.; Cherrington, B.D.; Xu, B.; Liu, X.; Zhang, X. Decreased microRNA-125b-5p disrupts follicle steroidogenesis through targeting PAK3/ERK1/2 signalling in mouse preantral follicles. *Metabolism* **2020** 107.
60. McAllister, J.M.; Han, A.X.; Modi, B.P.; Teves, M.E.; Mavodza, G.R.; Anderson, Z.L.; Shen, T.; Christenson, L.K.; Archer, K.J.; Strauss, J.F. miRNA Profiling Reveals miRNA-130b-3p Mediates DENND1A Variant 2 Expression and Androgen Biosynthesis. *Endocrinology* **2019**, 160, 1964-1981.
61. Kulkarni, R.; Teves, M.E.; Han, A.X.; McAllister, J.M.; Strauss 3rd, J.F. Colocalization of Polycystic Ovary Syndrome Candidate Gene Products in Theca Cells Suggests Novel Signaling Pathways. *J Endocor Soc* **2019**, 3, 2204-2223.

 doi:10.20944/preprints202404.0003.v1

62. Waterbury, J.S.; Teves, M.E.; Gaynor, A.; Han, A.X.; Mavodza, G.; Newell, J.; Strauss 3rd, J.F.; McAllister, J.M. The PCOS GWAS Candidate Gene ZNF217 Influences Theca Cell Expression of DENND1A.V2, CYP17A1, and Androgen Production. *J Endocor Soc* **2022**, 6.
63. Lv, M.; Zhong, Z.; Chi, H.; Huang, M.; Jiang, R.; Che, J. Genome-Wide Screen of miRNAs and Targeting mRNAs Reveals the Negatively Regulatory Effect of miR-130b-3p on PTEN by PI3K and Integrin β1 Signaling Pathways in Bladder Carcinoma. *Int J Mol Sci* **2016**, 18, 78.
64. Gioacchini, G.; Notarstefano, V.; Sereni, E.; Zacà, C.; Coticchio, G.; Giorgini, E.; Vaccari, L.; Carnevali, O.; Borini, A. Does the molecular and metabolic profile of human granulosa cells correlate with oocyte fate? New insights by Fourier transform infrared microspectroscopy analysis. *Mol Hum Reprod* **2018**, 24, 521-532.
65. Pangas, S.A. Bone morphogenetic protein signaling transcription factor (SMAD) function in granulosa cells. *Mol Cell Endocrinol* **2012**, 356, 40-47.